



RESEARCH ARTICLE

Marine aerosol generation experiments in the High Arctic during summertime

Jessica A. Mirrielees¹, Rachel M. Kirpes¹, Emily J. Costa¹, Grace C. E. Porter^{2,3}, Benjamin J. Murray², Nurun N. Lata⁴, Vanessa Boschi⁵, Swarup China⁴, Amanda M. Grannas⁵, Andrew P. Ault¹, Patricia A. Matrai^{6,*} , and Kerri A. Pratt^{1,7,*} 

The rapidly warming Arctic has transitioned to thinner sea ice which fractures, producing leads. Few studies have investigated Arctic sea spray aerosol (SSA) produced from open ocean, leads, and melt ponds, which vary in salinity and organic and microbial community composition. A marine aerosol reference tank was deployed aboard an icebreaker to the Arctic Ocean during August–September 2018 to study SSA generated from locally collected surface waters. Aerosol generation experiments were carried out using water collected from the marginal ice zone, a human-made hole in sea ice near the North Pole, and both lead and melt pond water during an ice floe drift period. Salinity, chlorophyll *a*, organic carbon, nitrogen, and microbial community composition were measured. Eukaryotic plankton and bacterial abundance were elevated in experimental water from the marginal ice zone, but the relative contributions from major eukaryotic taxonomic groups varied little across the experiments. The chemical composition of individual SSA particles was analyzed using Raman microspectroscopy and computer-controlled scanning electron microscopy with energy-dispersive X-ray spectroscopy. Individual sea salt aerosol, primary organic aerosol, and mineral dust particles were observed. Sea salt aerosol constituted 44–95% of individual submicrometer and 68–100% of supermicrometer particles, by number, generated during each experiment. Carbon was detected in 85%, by number, of the individual sea salt particles, with visible organic coatings. Carbohydrates were detected in 72% of particles, by number, with smaller contributions from long-chain fatty acids (13%) and siliceous material (15%). SSA generated from melt pond water contained only long-chain fatty acids and siliceous material. Quantification of the ice-nucleating activity showed that locally produced SSA may define the High Arctic background ice-nucleating particle population, but cannot account for the peak atmospheric concentrations observed. As the Arctic warms, the increasing SSA emissions have a complex dependence on changing biological and physical processes.

Keywords: Arctic, Aerosols, Air-ice-sea, Microbiology, Chemical composition, Single-particle

1. Introduction

Aerosol particles produced from seawater, known as sea spray aerosol (SSA), represent the largest global aerosol

flux to the troposphere (de Leeuw et al., 2011). SSA is produced primarily by a wave-breaking mechanism in which bubbles rise through the water column and break through the sea surface to release droplets into the air (Quinn et al., 2015; Russell et al., 2023). SSA particles consist of sea salt, organics, and often a combination thereof (Prather et al., 2013; Quinn et al., 2015; Russell et al., 2023). SSA particles can participate in cloud formation by acting as cloud condensation nuclei (Quinn et al., 2015; Christiansen et al., 2020; Ickes et al., 2020) and ice-nucleating particles (INPs; DeMott et al., 2016; Vergara-Temprado et al., 2017; Alpert et al., 2022). Studies have shown that SSA may be a particularly important source of INPs in the High Arctic (Bigg and Leck, 2001; Vergara-Temprado et al., 2017; Wex et al., 2019; Ickes et al., 2020; Wagner et al., 2021; Creamean et al., 2022). The component of SSA that causes ice nucleation is thought to be organic material related to biological activity in the ocean (Wang et al., 2015; Wilson et al., 2015; DeMott et al.,

¹ Department of Chemistry, University of Michigan, Ann Arbor, MI, USA

² School of Earth and Environment, University of Leeds, Leeds, UK

³ School of Physics and Astronomy, University of Leeds, Leeds, UK

⁴ Environmental Molecular Sciences Laboratory, Pacific Northwest National Laboratory, Richland, WA, USA

⁵ Department of Chemistry, Villanova University, Villanova, PA, USA

⁶ Bigelow Laboratory for Ocean Sciences, East Boothbay, ME, USA

⁷ Department of Earth and Environmental Sciences, University of Michigan, Ann Arbor, MI, USA

* Corresponding authors:

Emails: prattka@umich.edu; pmatrai@bigelow.org

2016; Irish et al., 2017; McCluskey et al., 2018; Zeppenfeld et al., 2019; Ickes et al., 2020).

Rapid warming in the Arctic (Pachauri et al., 2014; Overland et al., 2019) is reducing sea ice cover (Johannesen et al., 1999; Comiso, 2002; Overland and Wang, 2013), with thick, multi-year ice transitioning to thinner, first-year ice (Richter-Menge and Farrell, 2013). In the Arctic, areas of open water known as leads are created when fractures form in sea ice (Richter-Menge and Farrell, 2013). Leads act as a source of Arctic SSA via wind-driven processes (Scott and Levin, 1972; Radke et al., 1976; Nilsson et al., 2001; Leck et al., 2002; May et al., 2016b; Kirpes et al., 2019; Chen et al., 2022), as well as other bubble formation processes that may be important under low wind speed conditions, such as the bursting of gas bubbles released from melting sea ice (Nilsson et al., 2001) and the bursting of gas bubbles emitted by marine microbes during cellular respiration (Johnson and Wangersky, 1987). The year-round production of SSA from leads has been documented at a coastal Arctic site (May et al., 2016b). This observation suggests the potential for year-round SSA production across the entire Arctic region, especially with increasing thinner, first-year ice cover that is more prone to fracturing than multi-year ice (Qu et al., 2021; Sumata et al., 2023). Additionally, during late spring and summer, first-year ice is covered more extensively by melt ponds (pools of water that form when the top layer of the snow and sea ice melts) compared to multi-year ice (Stroeve et al., 2014). Transition to first-year ice is thus also expected to be increasing melt pond coverage in the Arctic. The potential for melt ponds to act as a source of SSA was investigated by Dall'Osto et al. (2017), who reported SSA generation experiments using melted Antarctic sea ice; however, we are not aware of any other related studies of aerosol generation from melt ponds. With sea ice loss, increasing open water, and increasing melt pond coverage, a corresponding increase in SSA production is likely affecting the radiative balance in the Arctic (Struthers et al., 2011; Browse et al., 2014). These significant changes in the Arctic Ocean make the study of SSA produced from open water, leads, and melt ponds critical for our understanding of Arctic climate and its impacts on global climate.

Numerous studies have measured the chemical composition of SSA in the Arctic (e.g., Hara et al., 2002; Leck et al., 2002; Bigg and Leck, 2008; Leck et al., 2013; Frossard et al., 2014; Chi et al., 2015; Willis et al., 2018; Kirpes et al., 2019; Zeppenfeld et al., 2023). SSA particles are often enriched in organic carbon compared to seawater (Hoffman and Duce, 1976; Prather et al., 2013). In the Arctic, organic coatings have been observed on individual sea salt aerosol particles (Bigg and Leck, 2008; Hawkins and Russell, 2010; Kirpes et al., 2019), with thicker coatings measured when sea ice leads were present, compared to open water (Kirpes et al., 2019). These coatings can consist of polysaccharides (Kirpes et al., 2019), which previous Arctic studies show are enriched in the sea surface microlayer and in SSA relative to the bulk seawater (Gao et al., 2012; Zeppenfeld et al., 2023). Organic matter in seawater can exist in the form of marine microgels, which

are polymer networks formed by cross-linking of organic material (Chin et al., 1998; Verdugo, 2012; Orellana and Leck, 2015). These polymer gels are a primary source of polysaccharides in SSA (Leck et al., 2013). Fatty acids have also been identified in Arctic SSA particles (Kirpes et al., 2019; Siegel et al., 2021), and the enrichment of fatty acids has been observed in both the sea surface microlayer and SSA (van Pinxteren et al., 2023). Marine microgels are stabilized by divalent calcium and magnesium ions (Chin et al., 1998; Verdugo, 2012; Orellana and Leck, 2015; Xu et al., 2016). As a result, SSA particles enriched in organics are also often enriched in calcium (Keene et al., 2007; Jayarathne et al., 2016) and/or magnesium (Jayarathne et al., 2016; Mukherjee et al., 2020) relative to seawater, as observed previously in the Arctic (Salter et al., 2016; Kirpes et al., 2019; Chen et al., 2022). Aerosolized marine microgels have the potential to facilitate Arctic fog and cloud formation (Orellana et al., 2021).

SSA can be studied under controlled conditions using a marine aerosol reference tank (MART), which consists of a closed tank that is partially filled with seawater, leaving a headspace above the seawater for SSA generation and sampling (Stokes et al., 2013). The water used in a MART experiment may be collected from a field site or produced artificially. Comparisons of SSA generation show that the plunging water jet and wave-breaking methods produce particle size distributions that are the most representative of ambient SSA (Fuentes et al., 2010; Prather et al., 2013; Collins et al., 2014). MART experiments are often used to study the relationship between the seawater microbiome and the properties of nascent SSA particles (Wang et al., 2015; Jayarathne et al., 2016; Cochran et al., 2017; Bertram et al., 2018; Hasenecz et al., 2020; Mayer et al., 2020), though few experiments have used seawater from the Arctic Ocean (Park et al., 2019a; Christiansen et al., 2020). The use of a MART to generate SSA provides the opportunity to study directly the composition of nascent SSA particles that have not undergone chemical reactions or mixing with advected air masses.

Ten MART SSA generation experiments were carried out during the Microbiology-Ocean-Cloud-Coupling in the High Arctic (MOCCHA) campaign aboard the Swedish Icebreaker (I/B) *Oden* in August–September 2018. Experimental waters were collected from the marginal ice zone (MIZ), a human-made hole in the sea ice near the North Pole, and both lead and melt pond water during an ice floe drift period. Each locally collected water sample was used in an aerosol generation experiment to assess potential connections between the marine microbial community and the physicochemical properties of individual nascent SSA.

2. Materials and methods

2.1. The MOCCHA campaign

The MOCCHA expedition began on August 1, 2018, when the I/B *Oden* departed from Longyearbyen, Svalbard (78.2°N, 15.6°E), and concluded when the *Oden* returned to Longyearbyen on September 22, 2018. This period included the end of the melt season (August 1–23), the transition into the autumn freeze-up period

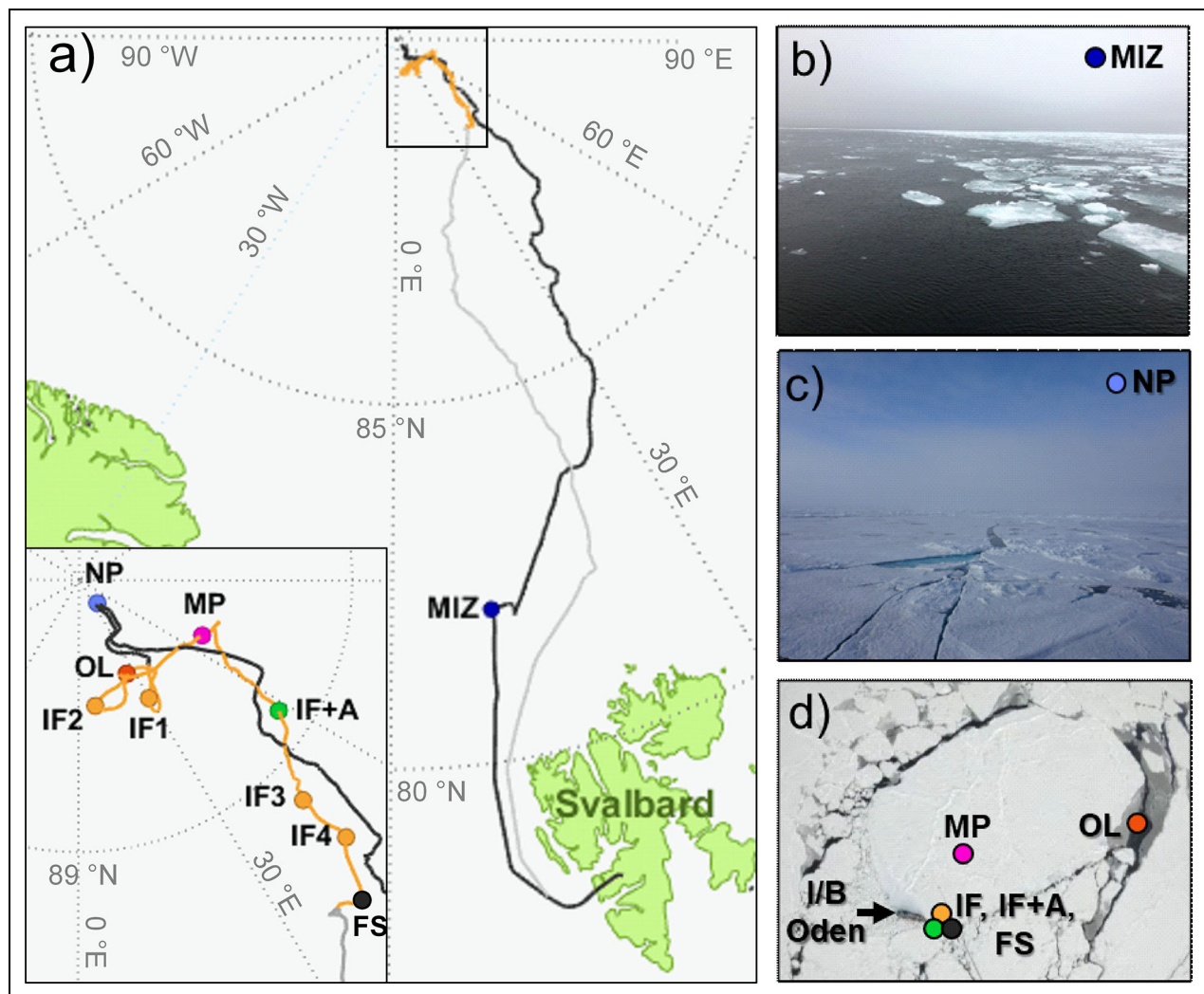


Figure 1. Cruise track and locations. (a) MOCCHA icebreaker cruise track from Svalbard to the ice floe station (dark gray line), along the ice floe drift path (orange line), and return journey to Svalbard (light gray line) (Prytherch and Tjernström, 2019). The inset provides a closer view of the ice floe drift path, including water sampling locations for the experiments described in **Table 1**. Photographs of (b) the marginal ice zone (MIZ) site, (c) the North Pole (NP) site, and (d) the sampling locations for the ice floe (IF) site (photo credit Paul Zieger), where the ice floe 1–4 (IF1–4), ice floe + added algae (IF+A), open lead (OL), and melt pond (MP) water samples were collected. The black arrow shows the location of the Icebreaker *Oden*.

(August 23–28), and the beginning of the autumn freeze-up period (August 28–September 22) (Vüllers et al., 2021). The cruise track for this expedition (Prytherch and Tjernström, 2019) and sampling site locations and photographs are shown in **Figure 1**. The *I/B Oden* passed into the MIZ, which is the transition zone between consolidated pack ice and the open ocean (Weeks, 2010), on August 8, 2018. After 24 hours at the MIZ, the *I/B Oden* continued northward until it reached a location near the North Pole (NP; **Figure 1c**) on August 12, 2018, where it moored for 8 hours. An ice floe suitable for long-term mooring of the *I/B Oden* was found at the location 89.605°N, 40.630°E. The ice floe measured approximately 0.6 km × 0.3 km, and was surrounded by leads on two sides. This ice floe served as an ice-drift station from August 14 to September 14, 2018 (**Figure 1d**), when it drifted approximately 120 km southward. Although seawater samples were collected at different depths, seawater was always collected

within the physical mixed layer that persisted at approximately 0–20 m for most of the drift and 0–40 m toward the end of the drift (Schanke et al., 2020). Geographical difference, due to the southward drift, and seasonal difference (summer melt period versus fall with freeze onset; Vüllers et al., 2021) likely may be stronger than depth-related variability.

A total of 10 aerosol generation experiments were carried out using the MART (Stokes et al., 2013). The total number of MART experiments was limited by the duration of each experiment (approximately 60 hours), plus the 12–24 hours required for experimental setup and water collection and 12 hours required for MART cleaning between experiments. A summary of the surface water sampling details for each of the MART experiments is given in **Table 1**, with a brief description of each location provided here. Water collection was accomplished using a rosette with a conductivity-temperature-depth (CTD)

Table 1. Summary of MART experiments, corresponding surface water sampling details and initial water temperature for each experiment

Experiment	Collection Date	Latitude (°N)	Longitude (°E)	Sampling Method	Depth (m)	MART Water Temperature ^a (°C)
Marginal ice zone (MIZ)	Aug 2	82.2	9.9	CTD	3	6 ± 2
North Pole (NP)	Aug 12	89.9	38.1	CTD	5	2.7 ± 0.5
Ice floe exp 1 (IF1)	Aug 17	89.5	30.6	Niskin bottle	5	5 ± 2
Ice floe exp 2 (IF2)	Aug 22	89.5	7.5	Niskin bottle	8	3.3 ± 0.8
Ice floe exp 3 (IF3)	Sep 7	88.9	45.6	Niskin bottle, pump	8	1.1 ± 0.5
Ice floe exp 4 (IF4)	Sep 10	88.7	46.2	CTD	8	1.2 ± 0.3
Ice floe + algae (IF+A)	Sep 3	89.8	54.1	Niskin bottle, pump	8	0.8 ± 0.4
Open lead (OL)	Aug 26	89.6	27.0	Bucket	0.6	-0.1 ± 0.2
Melt pond (MP)	Aug 30	89.5	65.8	Bucket	0.6	3 ± 1
Filtered seawater below ice floe (FS) ^b	Sep 12	88.5	42.9	CTD	10	2 ± 2
	Sep 13	88.5	39.0	CTD	10	

^aThis temperature is the temperature of the surface water measured in the marine aerosol reference tank (MART) during the aerosol generation experiments, not the temperature at the time of collection.

^bThe FS experiment consisted of two water samples that were combined.

sensor and loaded with Niskin bottles, an underwater pump and/or single Niskin bottle, or by hand using a bucket (with a waist rope for safety), as noted. For the NP experiment, a hole was created in the sea ice for seawater sampling, as there was no naturally formed lead. During the drift period, surface seawater for the experiments was collected from the two leads located on opposite sides of the ice floe. Experimental waters obtained from the lead next to the icebreaker are labeled for the ice floe (IF1, IF2, IF3, IF4, and IF+A), and the experimental water obtained from the opposite lead is labeled for the open lead (OL). While the NP, IF1–4, and OL experiments consisted of surface seawater from within the pack ice, these experiments were given separate labels in order to acknowledge the differences in sampling locations and methods. The IF water collected on September 3 was inoculated with loose ice algal aggregates, obtained through an access hole cut in the sea ice, to perform a perturbation experiment to show the effects of ice algal material dominated by the diatom *Melosira arctica* on SSA (experiment IF+A). The IF waters collected on September 12 and 13 were filtered (0.2 µm Whatman high flow filter cartridge) to characterize SSA generated from filtered seawater (FS); they were pooled and used in the FS experiment. Surface water was also collected from a melt pond (MP) on the ice floe surface on August 30. The melt pond was approximately 1 m deep at its center, 4 m wide at its widest point, and was not connected to the ocean at the bottom. It was filled with clear water, turquoise in color, and devoid of visible aggregates.

2.2. MART with plunging jet

The experiments were carried out using a MART (Stokes et al., 2013) with dimensions of 92 cm × 46 cm × 51 cm

(Figure S1). The total volume of the MART is 210 L, and it was filled with 100 L of collected surface water during each experiment, leaving a headspace of 110 L. Prior to the MOCCHA expedition, bubble size spectra were measured within the MART, using cold seawater from the Gulf of Maine during a set of SSA generation experiments in January 2018 (Mirrielees et al., 2022), and optimized to spectra previously determined for wave breaking in cold seawater (Brooks et al., 2009; Norris et al., 2011). The MART was sequentially rinsed with milli-Q water and sample water between experiments. Aerosol particles were generated using a waterfall cycle (4 seconds on, 4 seconds off), with 4.5 minutes per cycle and 0.5 minutes between cycles (AMT pump 368000180). In order to maintain a low water temperature representative of the surface seawater, the water in the tank was continuously cycled through chilling coils, and the MART itself was located outdoors on the deck of the ship to take advantage of the low ambient air temperature. Before the MART waterfall was started for each experiment, the tank was purged with particle-free air until the aerosol number concentration fell below 10 cm⁻³.

2.3. Surface water measurements

Salinity and concentrations of chlorophyll *a*, dissolved organic carbon (DOC), and dissolved organic nitrogen (DON) were measured for each of the 10 MART experiments. Measurements of particulate organic carbon (POC), particulate nitrogen (PN), and abundances of eutrophic pico-nanoplankton, heterotrophic nanoplankton, and bacteria were carried out for all but the FS experiment. DOC and total dissolved nitrogen (TDN) were analyzed using a Shimadzu TOC-L system equipped with TNM-L (total nitrogen measurement with chemiluminescence

detection), following a previously described method (Dickson et al., 2007) with calibration reference material provided by the Hansell Consensus Reference Material program (Hansell, 2005). The measured TDN mostly consisted of DON (Schanke et al., 2020) and is hereon denoted as DON. For each experiment, measurements of DOC and DON concentration were conducted for 2–4 subsamples drawn from a 60 mL water sample, and the means and standard deviations were calculated from the replicates. Chlorophyll *a* samples were collected on Whatman filters (GF/F grade, 0.7 μm), extracted in 90% acetone, and analyzed using standard fluorometric methods (Holm-Hansen et al., 1965; Welschmeyer, 1994). POC and PN samples were filtered on precombusted (450°C, 4 h) Whatman GF/F filters and frozen prior to analysis on a Costech Analytical Technologies ECS 4010 elemental analyzer (Steinberg et al., 2001). For each experiment, measurements of chlorophyll *a*, POC, and PN were conducted for 2–3 subsamples, and the means and standard deviations were calculated from the replicates. Practical salinity was determined from a calibrated Sea-Bird SBE 9 CTD (Bellevue, Washington) with a 24-bottle rosette on board the I/B *Oden*. Data from the down-casts were processed using the Seasave software (version 7.26.7.107). A hand-held (practical) salinity meter (Oakton, model SALT 6+) was used for discrete samples.

Samples were collected for 16S and 18S rRNA gene analysis on 0.2 μm Nucleopore membrane filters. Following collection, these samples were immediately frozen in liquid nitrogen and stored at -80°C until DNA extraction. Samples were extracted and purified with DNeasy[®] PowerWater[®] (Qiagen), and sent to the Integrated Microbiome Resource (IMR) at Dalhousie University (Halifax, Canada) for gene amplification, sequencing, and community composition assignments (Comeau and Kwawukume, 2023). Taxonomic classification was assigned using the Microbiome Helper pipeline (https://github.com/LangilleLab/microbiome_helper/wiki), based on QIIME2, that uses amplicon sequence variants (ASVs), specifically the universal V4–V5 amplicon sequencing primers (e.g., 515FB forward, 926R reverse primers for 16S sequences), created with Deblur (Comeau et al., 2017). Operational taxonomic units (OTUs) were then grouped mostly at the phylum level, following the National Center for Biotechnology Information (NCBI) Taxonomy Browser (<https://www.ncbi.nlm.nih.gov/>).

The abundance of phytoplankton was also quantified for each experiment via flow cytometry at the Bigelow Center for Aquatic Cytometry (CAC, East Boothbay, ME, USA), using a BD FACS Jazz/Influx Mariner (Brussaard, 2004; Marie et al., 2005). Samples were preserved with 10% paraformaldehyde and stored at -80°C until analysis (Vaulot et al., 1989; Poulton, 2023). Bacterial cells were stained using the DNA stain SYBR Green I (ThermoFisher Scientific) prior to analysis. Flow cytometry was used to enumerate eutrophic nanoplankton (cells 2–20 μm diameter) and picoplankton (cells 0.2–2 μm diameter), as well as heterotrophic nanoplankton (cells 2–20 μm diameter; Christaki et al., 2011) and bacteria (Vaulot et al., 1989; Durand and Olson, 1996; Lomas et al., 2010).

2.4. MART aerosol particle collection and analysis

The size distribution of the generated aerosol particles was measured every 5 minutes, and aerosol particles were sampled for subsequent analysis, for a duration of 6 hours for each experiment. After this 6-hour period, aerosol particles were sampled using cascade impactors for 48 hours (data not shown herein), followed by 0.5-hour sampling for final aerosol size distribution measurements, and then by a 0.5-hour bioaerosol sampling period (data not shown herein). MART experimental air was passed through two diffusion driers to maintain an aerosol flow relative humidity (RH) of approximately 15%. MART aerosol size distributions were measured with a scanning mobility particle sizer (SMPS model 3938, TSI Inc., sample flow rate 0.35 LPM, sheath flow rate 3.0 LPM, 14.1–736.5 nm d_m , mobility diameter) and an aerodynamic particle sizer (APS, model 3321, TSI Inc., sample flow rate 1.0 LPM, sheath flow rate 4.0 LPM, 0.523–19.81 μm d_a , aerodynamic diameter). The size distributions from the SMPS and the APS were merged, with an assumed shape factor of 1 and particle density of 2.0 g cm^{-3} (Khlystov et al., 2004).

Aerosol particles were sampled from the MART (for all experiments, except the FS experiment) using a 10-stage rotating micro-orifice uniform deposit impactor (MOUDI, model 120R, MSP Corp.). The total flow rate to the MOUDI (30 LPM) consisted of 3.5 LPM of air sampled from the MART headspace and an additional 26.5 LPM of particle-free air (filtered with a 1.2 μm pore size HEPA capsule, Pall Life Sciences). The MOUDI collected particles on transmission electron microscopy (TEM) grids, silicon, and quartz (Ted Pella, Inc.) on four stages ($<0.056 \mu\text{m}$ d_a , 0.10–0.18 μm d_a , 0.32–0.56 μm d_a , and 1.0–1.8 μm d_a) for subsequent offline single-particle analysis (see Sections 2.4.1 and 2.4.2). Following particle collection, the TEM grid, silicon, and quartz samples were stored in the dark at room temperature (Laskina et al., 2015). For several MART experiments, six of the remaining MOUDI stages (0.056–0.10 μm d_a , 0.18–0.32 μm d_a , 0.56–1.0 μm d_a , 1.8–3.2 μm d_a , 3.2–5.6 μm d_a , and 5.6–10 μm d_a) were loaded with polycarbonate filters (0.4 μm pore size, Nucleopore Track-Etched Membrane) for determination of the INP concentrations (see Section 2.4.3). The polycarbonate samples were stored at 4°C prior to INP analysis, which took place within 1–4 days of atmospheric particle collection.

2.4.1. Scanning electron microscopy with energy-dispersive X-ray spectroscopy

Computer-controlled scanning electron microscopy with energy-dispersive X-ray spectroscopy (CCSEM-EDX) was used to analyze individual particles from all MART experiments, with the exception of the FS experiment. The particles analyzed using CCSEM-EDX were collected onto TEM grids and silicon, on the MOUDI stages corresponding with the d_a ranges of 0.1–0.18 μm , 0.32–0.56 μm , and 1.0–1.8 μm . Analysis of particles collected on TEM grids is optimal for determination of elemental composition due to low background signal from the substrate, while the silicon substrate enables better quantitation of carbon. CCSEM-EDX analysis was carried out on 39,953 particles

collected on TEM grids, and 12,674 particles collected on silicon (Figure S2). Particle types were quantified as the fraction of the total number analyzed and its error ($= \sqrt{[F(1-F)/N]}$).

An FEI Quanta environmental scanning electron microscope (SEM) with a field emission gun operating at an accelerating voltage of 20 kV and beam current 0.48 nA was used for the CCSEM-EDX analysis. A scanning transmission electron microscopy high angle annular dark field (STEM HAADF) detector was used to analyze particles collected on TEM grids, while a secondary electron detector (Everhart-Thornley) was used to analyze particles collected on silicon wafers. An EDX spectrometer (EDAX, Inc.) was used to collect X-ray spectra and quantify the relative atomic abundance of the elements C, N, O, Na, Mg, Al, Si, P, S, Cl, K, Ca, Ti, V, Fe, Ni, and Zn for particles collected on TEM grids, with all elements except Si analyzed for the particles collected on silicon wafers.

K-means clustering was used to group the 39,953 individual particle (TEM grid) EDX spectra into 20 clusters based on similarities in elemental composition, based on the established method described by Ault et al. (2012). This number of clusters was chosen to account for potential small variations in elemental composition, as the error analysis of the clusters showed that only 5 clusters were required. These clusters were subsequently combined into three particle types which have previously been observed in SSA: sea salt particles dominated by sodium and chlorine (Ault et al., 2013a; Ault et al., 2013b; Prather et al., 2013; Wang et al., 2015), organic aerosol particles containing only carbon and oxygen (Prather et al., 2013; Wang et al., 2015), and mineral dust particles dominated by oxygen, as well as aluminum and/or silicon (Cornwell et al., 2020). As indicated by organic coatings and carbon content (for particles collected on silicon), the particles classified as sea salt were primarily mixtures of sea salt and organics. Particles containing both sea salt and mineral dust were not observed in this study.

2.4.2. Raman microspectroscopy

Atmospheric particles collected on quartz were analyzed using a Horiba LabRAM HR Evolution spectrometer coupled with a confocal optical microscope (100× N.A. 0.9 Olympus objective), Nd:YAG laser (50 mW, 532 nm), and CCD detector using a 600 groove/mm diffraction grating. Raman spectra were collected over the 500–4000 cm^{-1} range with spectral resolution of approximately 1.8 cm^{-1} . The acquisition time for each Raman spectrum was 30 seconds, with three accumulations and a 20 second delay. In addition to manual Raman spectral data collection, an automated method for collecting Raman spectra, called computer-controlled Raman microspectroscopy (Craig et al., 2017), was used to increase throughput and to decrease user bias in the selection of individual particles. For each experiment, Raman spectra were collected for ≥ 10 individual particles each from two MOUDI stages (1.0–1.8 μm d_a and 0.32–0.56 μm d_a), for a total of 313 particles analyzed using Raman microspectroscopy. A χ^2 error analysis was carried out for the individual particle Raman spectra, in which each particle spectrum was

matched to one standard spectrum from a library of 64 Raman spectra collected from various saccharides, long-chain fatty acids, short-chain fatty acids, and amino acids/proteins (Cochran et al., 2017; Kirpes et al., 2019; Mirrielees et al., 2022). Each particle may have contained more than one class of organic compounds. The compound class matched to each particle represents its dominant compound class, and less prevalent components are not reported. The following analysis includes only individual particles with Raman spectra containing modes characteristic of organic compounds. While the goal of this analysis was the identification of classes of organic compounds in sea salt particles, sea salt particles (with organic components) cannot be differentiated from purely organic particles with high confidence using this technique, as sodium chloride is not Raman-active. However, as discussed in Section 3.4, a larger fraction of the generated atmospheric particles were identified as sea salt rather than organic-only.

2.4.3. Ice nucleation measurements (droplet freezing experiments)

Size segregated samples (0.056–0.10 μm d_a , 0.18–0.32 μm d_a , 0.56–1.0 μm d_a , 1.8–3.2 μm d_a , 3.2–5.6 μm d_a , and 5.6–10 μm d_a) collected using the MOUDI (Section 2.4) were analyzed using the $\mu\text{L-NIPI}$ (Nucleation by immersed particle instrument; Whale et al., 2015), the same technique that was employed for determining the INP content of ambient air samples during the MOCCHA expedition (Porter et al., 2022). The droplet freezing assays were done in a dedicated mobile laboratory (the IcePod) onboard the I/B *Oden* as soon as practically feasible after sampling (1–4 days). Prior to analysis the samples were stored in a refrigerator at +4°C. Briefly, the droplet freezing analysis involved placing the substrates in 5 mL of Milli-Q water (Millipore Alpha-Q, with a resistivity of 18 $\text{M}\Omega$ cm at 25°C) and mechanically agitating the sample using a vortex mixer in order to release the particles into suspension. These particle suspensions were then pipetted to make an array of about 40 droplets on a silanized glass slide (Hampton research) that was positioned on top of a cold stage. The cold stage was then cooled at a rate of 1°C minute^{-1} until all of the droplets had frozen. The cumulative fraction of droplets frozen as a function of temperature was then used to produce the INP concentration per unit volume of water of suspension and also per unit volume of air according to the equations set out in O'Sullivan et al. (2018). Blank experiments were run in which Milli-Q water that had not been exposed to particle-laden substrates was put through the same process as the samples. These blank experiments were performed on August 17, 22, and 24 and September 7 and 11 and were previously reported (Zinke et al., 2021).

3. Results and discussion

3.1. Surface water characterization

The salinity, concentrations of chlorophyll *a*, DOC, DON, POC, PN, and abundances of eutrophic pico-nanoplankton, heterotrophic nanoplankton, and bacteria in the water collected at each location were measured to provide

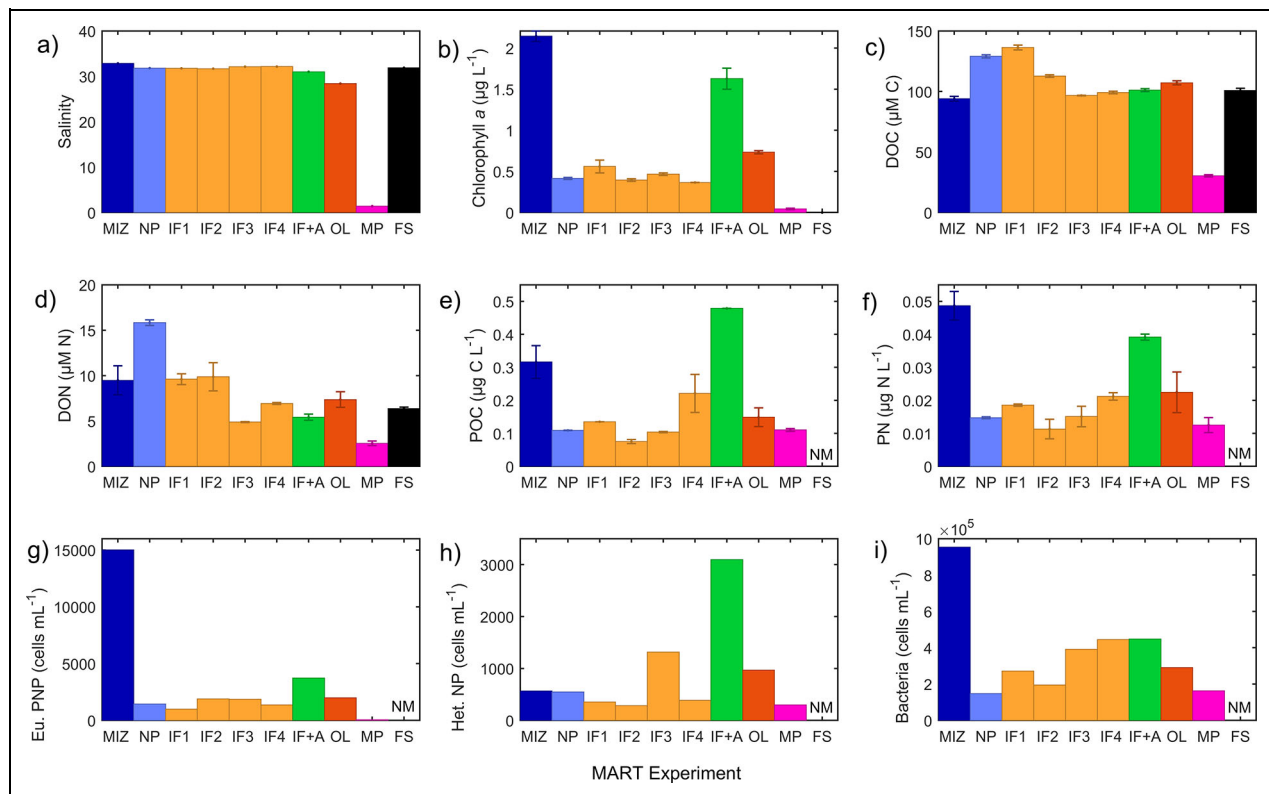


Figure 2. Characteristics of experimental water in the MART. Measurements of (a) salinity; average concentrations of (b) chlorophyll *a*, (c) dissolved organic carbon (DOC), (d) dissolved organic nitrogen (DON), (e) particulate organic carbon (POC), (f) particulate nitrogen (PN); and abundances of (g) eutrophic pico-nanoplankton (Eu. PNP), (h) heterotrophic nanoplankton (Het. NP), and (i) bacteria in water from each of the experiments, described in **Table 1**. No measurements (NM) were made for the filtered seawater (FS) experiment due to the removal of particulate matter. The error bars in (b)–(f) represent the standard deviations of 2–3 replicates (chlorophyll *a*, POC, PN) or 2 replicates (DOC, DON). The DON measurements presented here reflect the concentration of total dissolved nitrogen, which mostly consisted of DON (Schanke et al., 2020) and is hereon denoted DON.

context for the corresponding generated SSA. The surface water results are summarized in **Figure 2**. The measured chlorophyll *a* and DOC concentrations agree with previous summertime High Arctic Ocean measurements of $\leq 1.5 \mu\text{g L}^{-1}$ (Ardyna et al., 2013; Creamean et al., 2022) and 34.4–225 μM (Wheeler et al., 1997; Bussmann and Kattner, 2000), respectively. However, the DON concentrations (average, standard deviation) measured in the MIZ ($10 \pm 2 \mu\text{M}$, $n = 2$ subsamples), NP ($15.8 \pm 0.3 \mu\text{M}$, $n = 2$ subsamples), IF1 ($9.6 \pm 0.6 \mu\text{M}$, $n = 2$ subsamples), and IF2 ($10 \pm 2 \mu\text{M}$, $n = 2$ subsamples) experimental waters were higher than previous summertime High Arctic Ocean measurements of approximately 5–7 μM (Letscher et al., 2013). The POC and PN concentrations in the current study (0.075 – $0.5 \mu\text{g L}^{-1}$ and 0.011 – $0.049 \mu\text{g L}^{-1}$, respectively) are within the ranges previously reported for seawater in the High Arctic Ocean (approximately 0.01 – $10 \mu\text{g L}^{-1}$ and approximately 0.001 – $1 \mu\text{g L}^{-1}$, respectively) from February to July (Huang et al., 2018). The MIZ water was characterized by high salinity, chlorophyll *a*, POC, and PN concentrations, as well as the largest abundances of eutrophic pico-nanoplankton and bacteria of all the experimental waters. DOC and particularly DON concentrations were elevated in the NP water, a sample

that represents the northernmost newly broken sea ice encountered, rather than a naturally formed lead. The potential release of dissolved organic material (DOM) from sea ice biological processes within the newly opened brine channels could make a biogeochemical difference in the quantity and quality of DOM available for the formation of nascent aerosols. The surface water measurements were relatively consistent for the four IF samples, although elevated DOC and DON concentrations were measured during IF1 and IF2, and a greater abundance of heterotrophic nanoplankton was measured during IF3. A higher DON concentration in the NP sample was observed compared to the IF1–4 experimental waters, while the DOC (and POC and PN) concentrations were similar between the NP and IF1–4 experimental waters. The addition of ice algae to IF water for the IF+A experiment resulted in decreased salinity, increased concentrations of chlorophyll *a*, POC, and PN, and increased abundances of eutrophic pico-nanoplankton and heterotrophic nanoplankton compared to IF1–4. The OL water was less saline (28.4) than the IF experimental waters (31.7–32.1), likely due to the contribution of freshwater from the melting sea ice. The OL water was otherwise similar to the IF water, including with an elevated abundance of heterotrophic nanoplankton, similar

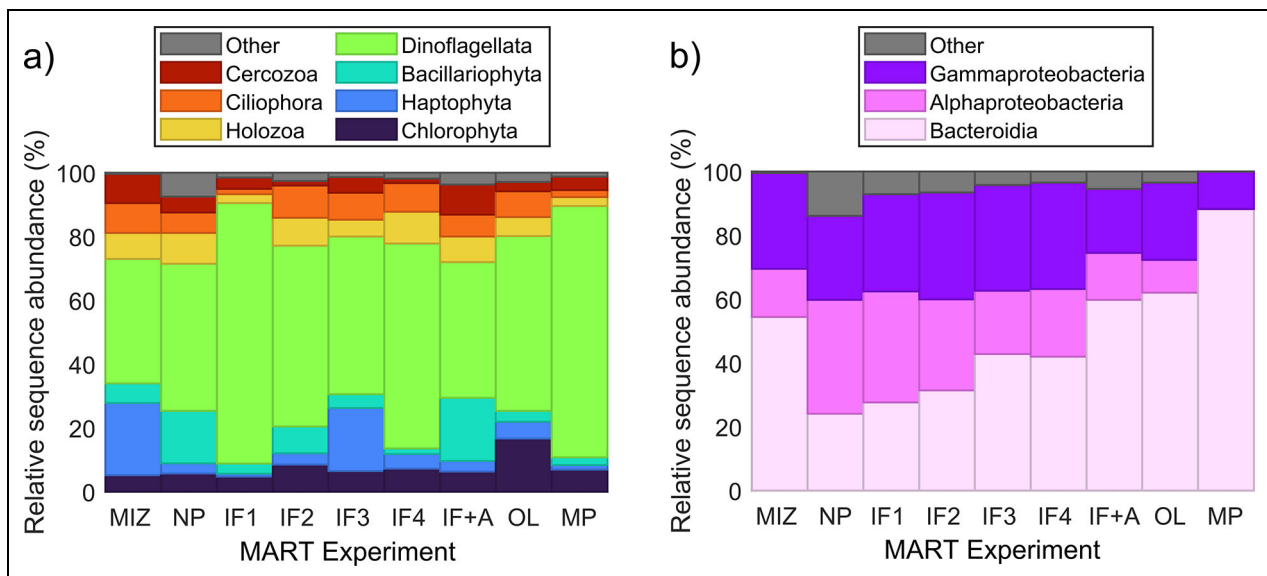


Figure 3. Plankton community composition in water from the MART experiments. Relative 16S or 18S rRNA gene sequence abundances of (a) eukaryotic and (b) prokaryotic taxa from the MART experiments, as described in **Table 1**. The group “Other” consists of additional taxonomic groups which were identified but accounted for less than 5% relative abundance across the nine unfiltered experimental waters.

to the IF3 experimental water. Salinity, DOC, and DON concentrations were similar between the FS experiment and the MIZ, NP, and IF1–4 experiments.

The MP water was characterized by the lowest salinity, as well as the lowest concentrations of chlorophyll *a*, DOC, and DON, of the collected experimental waters. The salinity measured at the MP site is consistent with salinity measurements from other melt ponds (Kim et al., 2018; Park et al., 2019b; Xu et al., 2020). The concentrations of chlorophyll *a* and DOC generally agree with those from prior studies on melt ponds (Galgani et al., 2016; Park et al., 2019b; Xu et al., 2020). Notably, the abundance of eutrophic pico-nanoplankton was lowest for the MP water, yet similar abundances of heterotrophic nanoplankton and bacteria were measured in the MP water and several of the IF waters.

The results of the 18S rRNA gene analyses are shown in **Figure 3a**. Seven major taxonomic groups were identified among the eukaryotes: Chlorophyta, Haptophyta, Bacillariophyta (including diatoms), Holozoa, Dinoflagellata, Ciliophora, and Cercozoa. Dinoflagellata was the dominant group observed with relative sequence abundances of 39–82%, with particularly high contributions to the IF1 and MP experiments of 82% and 79%, respectively. An analysis of phytoplankton pigments measured during the MOCCHA expedition found that photosynthetic dinoflagellates consistently accounted for <5% of the community (Schanke et al., 2020), which suggests that the dinoflagellates identified by the 18S rRNA gene analysis could be predominately heterotrophic. The difference in possible dinoflagellate dominance between the two methods could also be due to the high 18S rRNA gene copy number in dinoflagellates (Lin, 2011; Wisecaver and Hackett, 2011) biasing toward a high estimate of relative abundance.

The relative sequence abundances of several groups peaked for individual experimental waters, including Haptophyta in MIZ (23%) and IF3 (20%), Chlorophyta in OL (17%), and Bacillariophyta in NP (17%) and IF+A (20%). Bacillariophyta is a group that includes diatoms which have been found to dominate ice algal communities (Poulin et al., 2011; Assmy et al., 2013; Szymanski and Gradinger, 2016). These contributions by ice diatoms can be explained by the NP water being sampled from an opening made in sea ice by the research team, and by algae collected from loose sea ice algal mats being added for the IF+A water. The most abundant eukaryotic OTUs for each experiment, summarized in Table S1, showed little variance across the experiments. The results of the 18S analyses were used to calculate the Shannon-Wiener diversity index *H* (Table S2).

Prokaryotes were classified into three major taxonomic groups according to the 16S sequencing results: Bacteroidia, Alphaproteobacteria, and Gammaproteobacteria (**Figure 3b**). For the NP and IF1–4 experiments, no single taxonomic group accounted for a majority of the sequenced DNA; they were comprised of 24–42% Bacteroidia, 20–36% Alphaproteobacteria, and 26–34% Gammaproteobacteria. Bacteroidia was the dominant prokaryotic group in the remaining experiments, comprising 54–62% of the relative sequence abundance in the MIZ, IF+A, and OL experimental waters and 88% of the relative sequence abundance in the MP water. While Alphaproteobacteria accounted for 10–15% of the relative sequence abundances in the MIZ, IF+A, and OL experiments, only a negligible fraction (<0.2%) of Alphaproteobacteria was identified in the MP water. This lack of Alphaproteobacteria shows that the prokaryotic portion of the microbial community was distinct in the MP water compared to the seawater experiments. The dominant OTUs identified

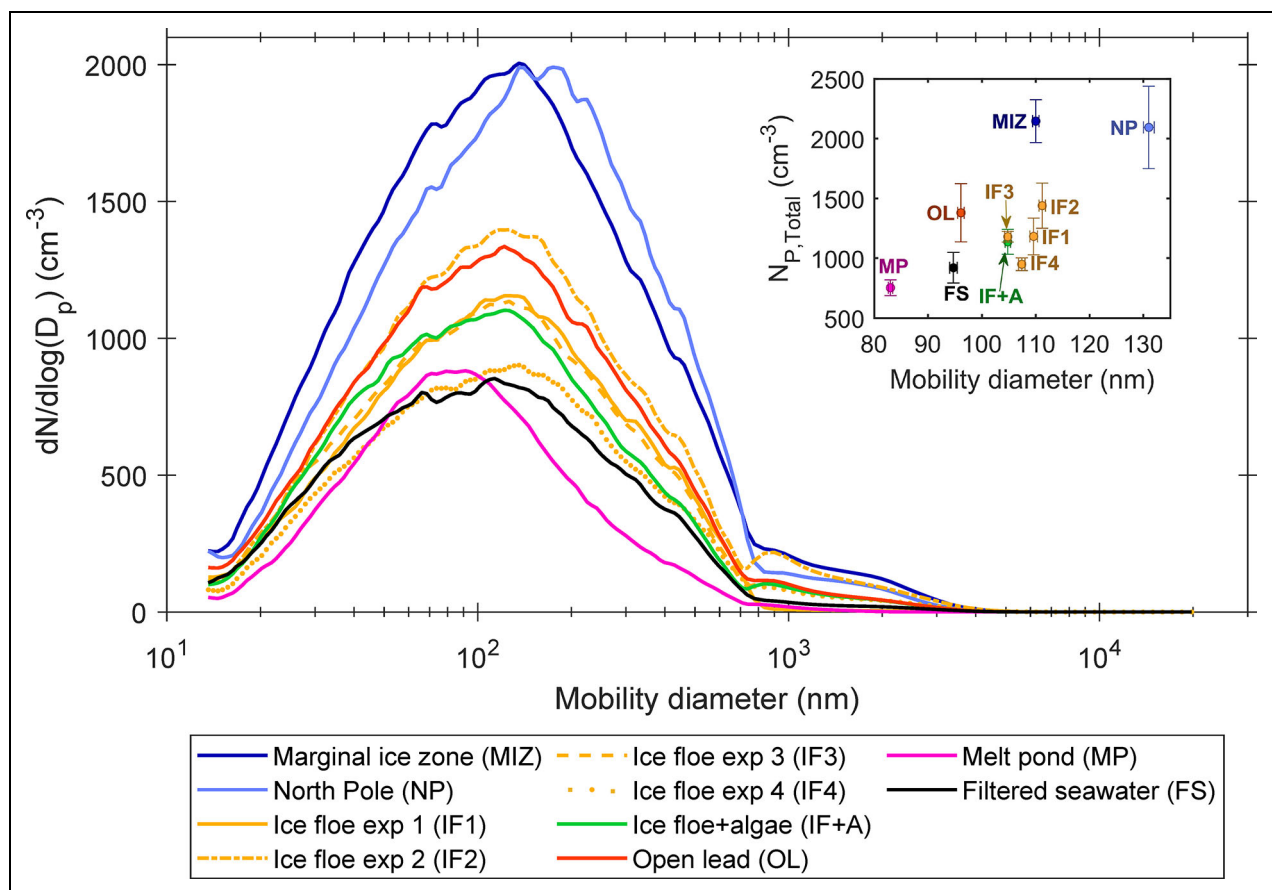


Figure 4. Average aerosol size distributions for the MART experiments. More details on each of the marine aerosol reference tank (MART) experiments indicated in the inset legend are provided in **Table 1**. The plotted distributions show aerosol particle concentrations measured by the scanning mobility particle sizer for particles in the range 13.6–737 nm d_m , and by the aerodynamic particle sizer in the range 0.777–20.0 μm d_m . The inset plot shows the mode diameter and total measured aerosol concentration for each experiment. The error bars represent the standard deviation for each location. Aerosol size distributions were measured every 5 minutes across 6 hours of each experiment; standard deviations across each size bin for each experiment are shown in Figure S3.

within the prokaryotic taxonomic groups during each experiment are summarized in Table S3.

3.2. Aerosol particle size distributions

The aerosol particle size distributions were similar for most of the MART experiments, each featuring two modes in the ranges of 83–131 nm and 1–2 μm (**Figures 4** and S2). Previous SSA generation experiments carried out using plunging jets (Hultin et al., 2010; Prather et al., 2013; Collins et al., 2014; Salter et al., 2015; May et al., 2016a; Schwier et al., 2017; Christiansen et al., 2019; Bates et al., 2020; Mirrielees et al., 2022) and breaking waves (Prather et al., 2013; Sauer et al., 2022) have resulted in SSA size distributions with modes of 90–200 nm. The aerosol particle size distribution from the NP experiment was characterized by the largest submicrometer mode (131 \pm 1 nm, standard deviation of the lognormal fit to the data) of the MART experiments. The salinity, chlorophyll *a* concentration, POC and PN concentrations, abundances of eutrophic pico-nanoplankton, heterotrophic nanoplankton, and bacteria, and relative abundance of taxonomic groups from the 16S and 18S sequence analyses were similar between the NP experiment and the other

experiments, which suggests that these factors do not explain the disparity in submicrometer mode among the MART experiments. Conversely, the concentration of DON in the NP experiment was markedly higher (by a factor of 1.6–6.2) compared to the other experiments. The highest total aerosol particle concentrations were measured during the NP (2100 \pm 300 cm^{-3} , standard deviation, $n = 72$) and MIZ (2100 \pm 200 cm^{-3} , standard deviation, $n = 80$) experiments. A two-sample Kolmogorov-Smirnov test showed no significant difference between the NP and MIZ aerosol size distributions.

The submicrometer SSA mode diameters for the MIZ, IF1–4, and IF+A experiments fell within a narrow range (105–111 nm; **Figure 4**). The submicrometer mode for the OL water (96 \pm 1 nm, standard deviation of the lognormal fit to the data) was similar to that for the FS water. Similar submicrometer modes have been observed previously in SSA generated from unfiltered seawater and filtered seawater, despite greater particle concentration from the unfiltered seawater (Tyree et al., 2007). The total aerosol particle concentration was higher for the OL experiment (1400 \pm 200 cm^{-3} , mean and standard deviation, $n = 74$) than the FS experiment (900 \pm 100 cm^{-3} , mean and

standard deviation, $n = 75$). Kolmogorov-Smirnov tests determined that the aerosol particle distributions measured during the IF1, IF3, and IF+A experiments could have arisen from the same underlying distribution ($p > 0.10$); the same conclusion was drawn for SSA generated during the IF2 and OL experiments ($p = 0.54$), and the IF4 and FS experiments ($p = 0.30$).

The lowest total aerosol particle concentration ($750 \pm 70 \text{ cm}^{-3}$; mean and standard deviation, $n = 73$) and smallest submicrometer mode diameter ($83 \pm 1 \text{ nm}$, standard deviation of the lognormal fit to the data) were measured for the MP experiment. The MP water had the lowest salinity (1.40) compared to the seawater experiments (28.4–32.84). The p -values calculated from Kolmogorov-Smirnov tests comparing the aerosol size distributions from the MP experiment with those from the IF4 ($p = 0.06$) and FS ($p = 0.08$) experiments are nearly low enough to consider the size distribution from the MP distinct from that of the other MART experiments. Note that the aerosol size distribution from the lower-salinity MP surface water is distinctly different from that of aerosol generated from Lake Michigan freshwater (May et al., 2016a), which was characterized by two modes (46 ± 6 and $180 \pm 20 \text{ nm}$) not observed in the MP SSA particle size distribution.

Studies on the effect of seawater temperature on SSA concentration have led to mixed results, with some experiments reporting a positive (Liu et al., 2021) or negative relationship between the two (Zábori et al., 2012a; Salter et al., 2014; Nielsen and Bilde, 2020), while others found that the two metrics were unrelated (Forestieri et al., 2018) or that the relationship between the two was complex (Mårtensson et al., 2003; Christiansen et al., 2019). No correlation was found between MART water temperature and total SSA concentration or mode diameter in this study. Some previous studies have reported that an increase in salinity results in an increase in SSA concentration (Rocchi et al., 2024) and mode diameter (Mårtensson et al., 2003; Tyree et al., 2007; Zábori et al., 2012b; Zinke et al., 2021). In contrast, other studies reported a decrease (Hultin et al., 2010; May et al., 2016a) or lack of change (Park et al., 2019a) in the mode diameter when salinity was increased. Here, the smallest SSA distribution mode diameter was observed during the MP experiment. However, the size distribution of SSA generated from the OL water was similar to the distributions observed in the other seawater experiments, despite a slightly lower salinity (28.4). Furthermore, while the lowest surface water salinity and lowest SSA concentration were both observed during the MP experiment, the SSA concentration was also low ($<1000 \text{ cm}^{-3}$) during the IF4 (salinity = 32.1) and FS (salinity = 31.8) experiments, which suggests that salinity was not the dominant factor in determining the total aerosol particle number concentration.

No statistically significant correlations were found between concentrations of chlorophyll a , POC, or PN, or the abundances of heterotrophic nanoplankton or bacteria and the total aerosol particle concentration or submicrometer mode diameter. However, total aerosol particle concentration correlated positively with both DON

concentration ($r^2 = 0.64$, $p < 0.01$) and abundance of eutrophic pico-nanoplankton ($r^2 = 0.41$, $p = 0.065$), while the SSA submicrometer mode diameter correlated positively with DOC concentration ($r^2 = 0.44$, $p = 0.037$) and DON concentration ($r^2 = 0.85$, $p < 0.01$). An increased concentration of dissolved organic compounds in seawater has been shown to result in increased SSA concentrations (Lv et al., 2020), and higher concentrations of dissolved glucose have been correlated with the concentration of $<200 \text{ nm}$ SSA (Rocchi et al., 2024). However, overall, the effects of marine bacteria and phytoplankton on SSA concentrations are not well resolved (Prather et al., 2013; Alpert et al., 2015; Park et al., 2019a; Dall'Osto et al., 2022). The lack of a clear relationship between the biological measurements and SSA concentrations likely stems from the complex nature of the microbial communities and their varying levels of extracellular release of DOM (Vernet et al., 2021) which also impacts SSA chemical composition, as described below.

3.3. Atmospheric single-particle elemental composition (CCSEM-EDX)

A total of 39,933 atmospheric particles collected on TEM grids using the MOUDI ($<0.056 \mu\text{m } d_a$, $0.10\text{--}0.18 \mu\text{m } d_a$, $0.32\text{--}0.56 \mu\text{m } d_a$, and $1.0\text{--}1.8 \mu\text{m } d_a$) were analyzed using CCSEM-EDX. The number of particles that were generated during each experiment and analyzed using CCSEM-EDX is shown in Figure S3. The elemental composition of the individual particles showed that sea salt particles, organic particles, and mineral dust particles were generated from the collected surface waters (Figure 5a–c). The dominant atmospheric particle type was sea salt (28,200 particles), which mostly consisted of sodium and chlorine, with sulfur, magnesium, and potassium present in small amounts. As shown from the particle analysis on silicon substrates, organics were present in many of the particles classified as sea salt. The inorganic portion of sea salt consists of common seawater ions (including sodium, chloride, magnesium, calcium, potassium, and sulfate), which are found throughout the ocean in consistent ratios (Millero et al., 2008). Sea salt particles accounted for 44–95%, by number, of the submicrometer ($0.1\text{--}1.0 \mu\text{m}$ projected area diameter) particles and 68–100% of supermicrometer ($1.0\text{--}8.7 \mu\text{m}$ projected area diameter) particles across the MART experiments. Previous studies of ambient (O'Dowd et al., 2004; Facchini et al., 2008; Gantt et al., 2011; O'Dowd et al., 2015; Kirpes et al., 2018; Kirpes et al., 2020) and laboratory-generated SSA (Facchini et al., 2008; Prather et al., 2013; Collins et al., 2014; Mirrielees et al., 2022) have also shown sea salt particles to dominate the supermicrometer SSA, while most organic particles are submicrometer. As expected based on the short residence time inside the MART headspace (Stokes et al., 2013), the sea salt particles showed no evidence of either chlorine depletion or sulfur and/or nitrogen enrichment indicative of secondary reactions (Laskin et al., 2002; Chi et al., 2015; Kirpes et al., 2018).

To assess SSA particle elemental composition, 12,674 sea salt particles collected on silicon ($0.10\text{--}0.18 \mu\text{m } d_a$, $0.32\text{--}0.56 \mu\text{m } d_a$, and $1.0\text{--}1.8 \mu\text{m } d_a$) were analyzed using

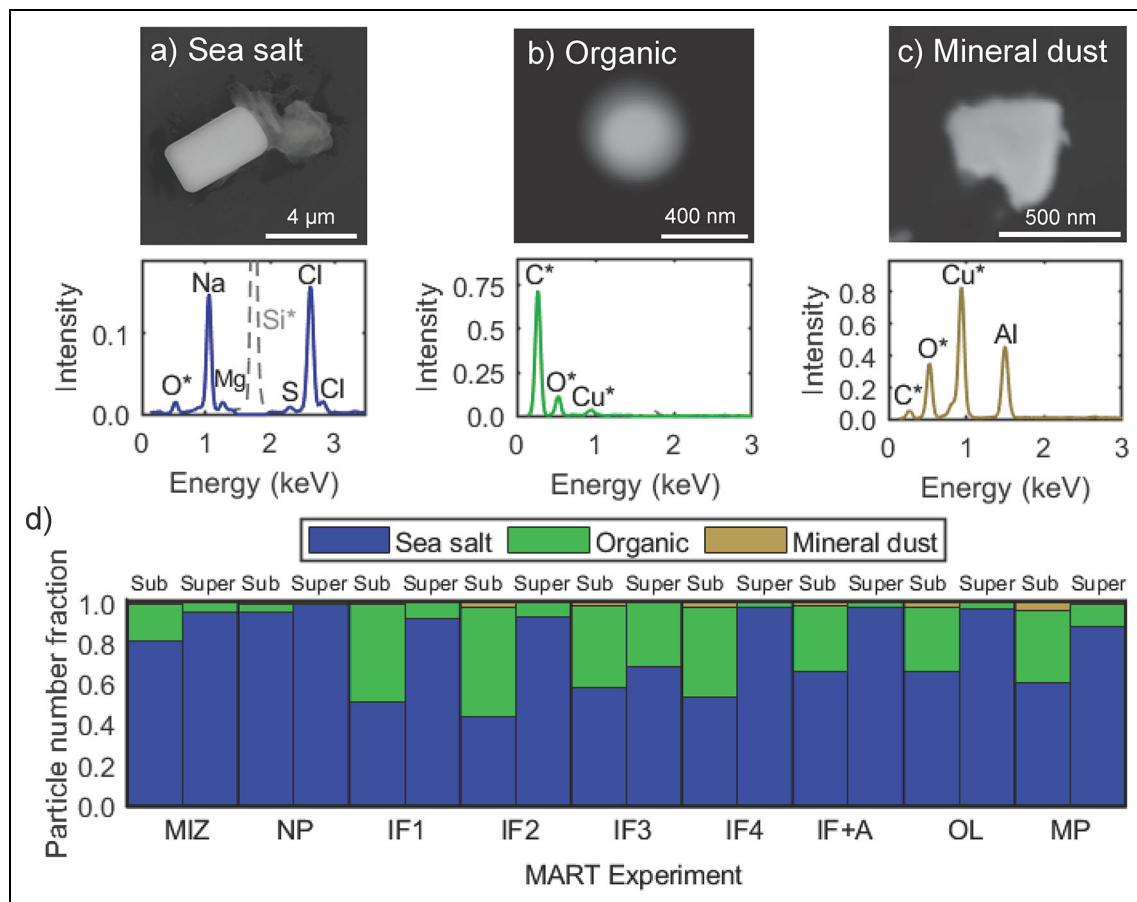


Figure 5. Characteristics of individual aerosol particles across all experiments. Representative scanning electron microscopy images and energy-dispersive X-ray (EDX) spectra of observed individual particle types including (a) sea salt aerosol, (b) organic aerosol, and (c) mineral dust particles. In (a), the sea salt particle was collected on silicon (peak removed for clarity) which allows for the quantification of organics (carbon and oxygen) in a particle. In the spectra of panels (b) and (c), particles were collected on transmission electron microscopy (TEM) grids, which contribute to the carbon, oxygen, and copper signals measured (*). The EDX detector also contributes to the silicon signal measured. Many of the EDX spectra from organic particles collected on TEM grids contain silicon peaks (Figure 5b), which are likely due to a minor silicon signal from the detector rather than the particle itself (Fraund et al., 2017). (d) Number fractions are shown for each observed individual particle type in the submicrometer (Sub) and supermicrometer (Super) projected area diameter ranges for each marine aerosol reference tank (MART) experiment.

CCSEM-EDX (Figure S3). An SEM image of several SSA particles (mostly sea salt particles) collected on a silicon wafer is shown in Figure S4. Carbon was detected in 81%, by number, of the submicrometer sea salt particles and 97%, by number, of the supermicrometer sea salt particles collected on silicon. These results further indicate that the particles classified as sea salt were primarily mixtures of sea salt and organics. The EDX spectra of sea salt particles collected on silicon were used to calculate the elemental mole ratios of each individual particle, including C/Na, Ca/Na, and Mg/Na (Figure 6), and Cl/Na, S/Na, and N/Na (Figure S5). Individual sea salt particles were enriched in organics relative to seawater, as indicated by elevated C/Na ratios (Figure 6a). For all experiments, greater carbon enrichment was measured in submicrometer sea salt particles ($C/Na = 0.27\text{--}0.41$) compared to supermicrometer sea salt particles ($C/Na = 0.061\text{--}0.14$), in agreement with previous measurements of Arctic sea salt aerosol particles (Kirpes et al., 2019). The highest C/Na

ratios (0.50–0.58) were observed during the IF1, IF2, and MP experiments, while the lowest C/Na ratios (0.25–0.30) were measured during the MIZ, IF3, and OL experiments. The measured C/Na ratios did not correlate with the concentrations of chlorophyll *a*, DOC, DON, POC, or PN or with the abundances of eukaryotic pico-nanoplankton, heterotrophic nanoplankton, or bacteria (Figure 2), which suggests that the enrichment of carbon in sea salt particles is influenced by additional factors beyond the quantity of carbon and nitrogen in the seawater, or the abundance of cells capable of producing organic exudates.

The Ca/Na and Mg/Na ratios were larger for submicrometer sea salt particles than supermicrometer sea salt particles (Figure 6). Calcium enrichment was greater in individual submicrometer sea salt particles ($Ca/Na = 0.16\text{--}0.36$) than supermicrometer sea salt particles ($Ca/Na = 0.029\text{--}0.1$), but both were enriched compared to the seawater ratio of 0.02 (Pilson, 2013). Calcium enrichment (elevated Ca/Na relative to seawater) has been

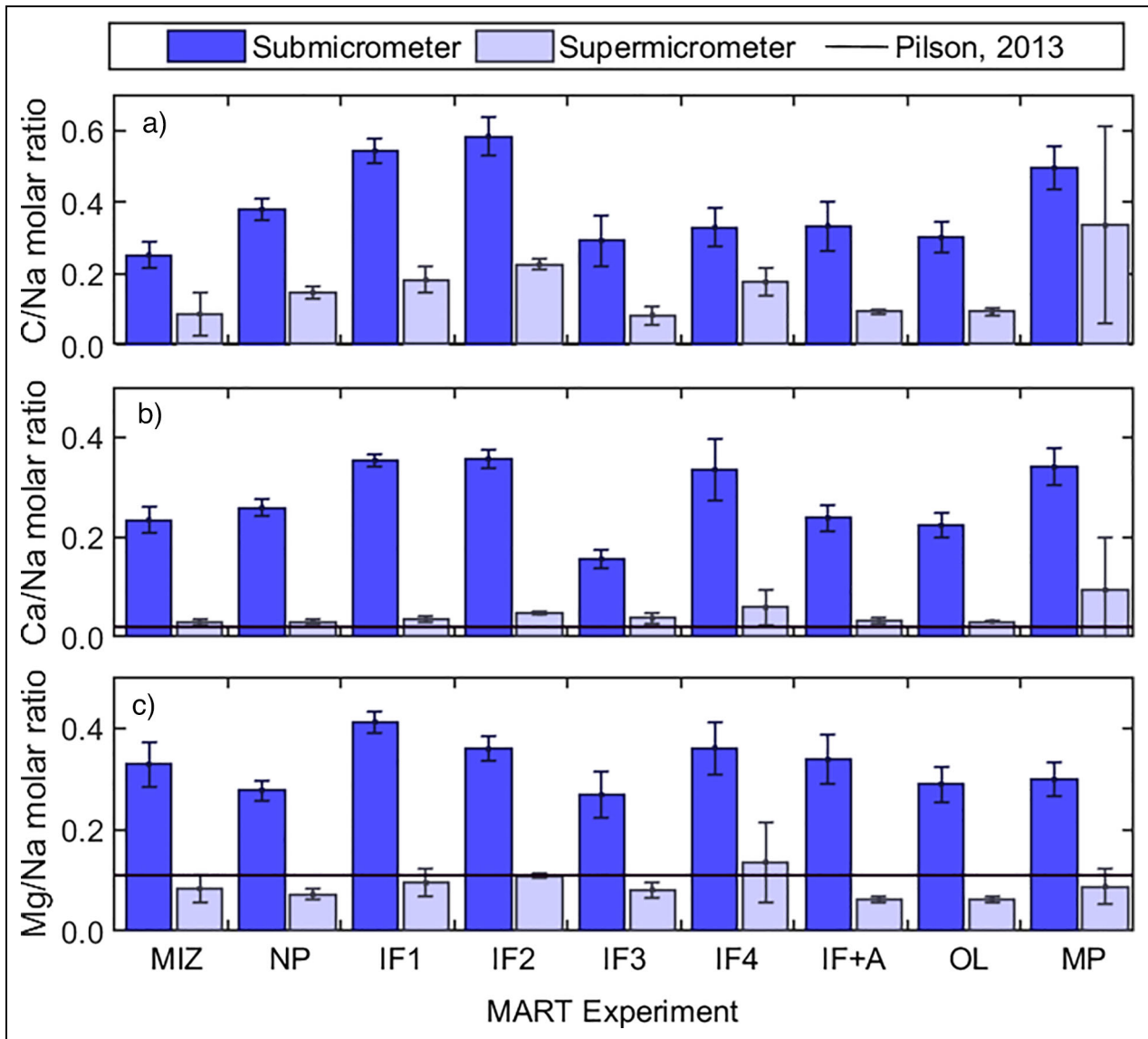


Figure 6. Mean elemental molar ratios of individual aerosol particles for each experiment. Mean (a) C/Na, (b) Ca/Na, and (c) Mg/Na molar ratios of individual sea salt particles (collected on silicon) for each marine aerosol reference tank (MART) experiment. Details of each MART experiment are provided in **Table 1**. Supermicrometer and submicrometer bins were based on projected area diameter, where each bin contains a minimum of 20 particles. Error bars represent the 95% confidence intervals for each mean. The horizontal lines indicate the elemental molar ratios for Ca/Na and Mg/Na in seawater (Pilson, 2013).

observed previously (Keene et al., 2007), with greater enrichment in smaller SSA particles (Cochran et al., 2016; Salter et al., 2016; Kirpes et al., 2019). Mg/Na ratios for individual submicrometer sea salt particles fell in the range of 0.27–0.41, also indicating magnesium enrichment relative to the seawater ratio of 0.11 (Pilson, 2013). Previous studies have shown slight (Kirpes et al., 2019) or negligible (Cochran et al., 2016; Salter et al., 2016) magnesium enrichment in submicrometer sea salt particles relative to seawater. In contrast, the Mg/Na ratios of supermicrometer sea salt particles generated from the MIZ, IF1, IF2, IF4, and MP experimental waters were similar to seawater. Further, supermicrometer sea salt particles generated from NP, IF3, IF+A, and OL experimental waters were depleted in magnesium relative to seawater:

0.07 ± 0.01 ($n = 720$), 0.062 ± 0.006 ($n = 146$), 0.061 ± 0.006 ($n = 190$), and 0.08 ± 0.02 ($n = 310$), respectively (95% confidence intervals). Previously reported Mg/Na ratios in supermicrometer SSA have been generally consistent with the seawater ratio (Salter et al., 2016; Kirpes et al., 2019), though some depletion has also been observed (Cochran et al., 2016). As discussed in the Introduction, Ca^{2+} ions (and Mg^{2+} ions to a lesser degree) stabilize polymer gels in seawater (Verdugo, 2012). The formation of complexes between organic material and these divalent cations provides a route for the aerosolization of sea salt aerosol particles enriched in carbon, calcium, and magnesium relative to seawater. The observation of larger C/Na, Ca/Na, and Mg/Na ratios in the individual submicrometer particles compared to the

individual supermicrometer particles in the current study (**Figure 6**) is consistent with the presence of organic gels stabilized by divalent cations. Greater enrichment in calcium compared to magnesium (**Figure 6**) is also consistent with previous SSA studies (Cochran et al., 2016; Salter et al., 2016; Kirpes et al., 2019). Discussion of the sea salt aerosol Cl/Na, S/Na, and N/Na ratios can be found in Text S1.

The remaining particles collected on TEM grids were classified as organic particles consisting of carbon and oxygen (11,246 particles), or as mineral dust particles consisting of aluminum and/or silicon, as well as oxygen (507 particles) (**Figure 5**). Organic particles accounted for 5–54%, by number, of the measured submicrometer particles and 0–32%, by number, of supermicrometer particles across the experiments. Previous studies have shown that the majority of organic particles produced by sea spray fall within the submicrometer range (Ault et al., 2013b; Prather et al., 2013; Kirpes et al., 2018), with which our results are consistent. Mineral dust accounted for 0–4%, by number, of the measured submicrometer particles and 0–1%, by number, of supermicrometer particles. The transfer of mineral dust particles from seawater to the aerosol phase via bubble bursting has been observed during previous seawater aerosol generation experiments (Cornwell et al., 2020). The origin of this dust within the seawater may be from suspended sediment from riverine sources (Ahmed et al., 2020) or sediment released from melting sea ice (Reimnitz et al., 1993; Nürnberg et al., 1994; Eicken et al., 1997; Measures, 1999; Darby et al., 2009; Darby et al., 2011; Klunder et al., 2012), and/or dust deposited at the ocean surface from atmospheric transport from high-latitude sources (Sanchez-Marroquin et al., 2020; Meinander et al., 2022; Barr et al., 2023).

Number fractions of particle types (sea salt, organic, and mineral dust) were generally consistent among the experiments (**Figure 5d**). However, larger number fractions of submicrometer sea salt particles were observed during the MIZ ($81.4\% \pm 0.6\%$, $n = 4356$; as defined in Section 2.4.1) and NP ($95.0\% \pm 0.3\%$, $n = 6269$) experiments, compared to the IF1–4 ($43.6\text{--}58\%$), IF+A ($65.8\% \pm 0.8\%$, $n = 3459$), OL ($66\% \pm 1\%$, $n = 1912$), and MP ($60.4\% \pm 0.9\%$, $n = 3011$) experiments. These observational differences are notable for three reasons. First, the surface water sampled from the MIZ was more biologically active than the surface waters collected at the IF site (IF1–4). The MIZ water was characterized by elevated chlorophyll *a* concentrations and greater abundances of eutrophic pico-nanoplankton and bacteria, compared to the IF1–4 experimental waters, as described in Section 3.1. Further, the NP and the IF1–4 experimental waters contained similar concentrations of chlorophyll *a*, POC, and PN, and similar abundances of eutrophic pico-nanoplankton, heterotrophic nanoplankton, and bacteria. Note that the lowest submicrometer and supermicrometer number fractions of organic particles were measured in the NP experiment, despite the relatively high DOC concentration in the NP water, which was only exceeded by the DOC concentration of the IF1 water. Lastly, the size distribution mode diameter was larger for the NP

experiment compared to the other MART experiments. The greater fraction of submicrometer SSA classified as sea salt in the NP experiment may explain this difference, as sea salt particles are generally larger than seawater-derived organic aerosol particles (Quinn et al., 2015).

The number fractions of supermicrometer sea salt aerosol were similar between the OL experiment ($97.1\% \pm 0.6\%$) and the IF1, IF2, and IF4 experiments ($92\text{--}97.8\%$), while the number fraction of submicrometer sea salt aerosol was higher in the OL experiment ($66\% \pm 1\%$) compared to the IF1, IF2, and IF4 experiments ($43.6\text{--}53\%$). The number fraction of submicrometer sea salt aerosol was also elevated in the IF3 experiment ($58\% \pm 1\%$) compared to the other IF experiments, but the number fraction of supermicrometer sea salt aerosol was much lower in the IF3 ($68\% \pm 2\%$) experiment compared to the other IF experiments, as well as the OL experiment. The number fraction of supermicrometer organic aerosol measured during the IF3 experiment ($32\% \pm 2\%$) was much higher than that measured during the IF1, IF2, IF4 ($2.2\text{--}8\%$) and OL experiment ($2.9\% \pm 0.6\%$). The increased number fraction of supermicrometer organic particles measured during the IF3 experiment may be explained by the higher abundance of heterotrophic nanoplankton in the IF3 water ($1316\text{ cells mL}^{-1}$) compared to the IF1, IF2, and IF4 experimental waters ($285\text{--}387\text{ cells mL}^{-1}$; **Figure 2**). Also notable is that the fraction of haptophytes was higher for the IF3 compared to the other IF experimental waters (**Figure 3**). This IF3 result points to the likely connection between the microbial community and marine organic aerosol generation.

Similar particle number fractions of sea salt were observed during the IF+A perturbation experiment (supermicrometer $97.1\% \pm 0.6\%$, $n = 658$; submicrometer $66\% \pm 1\%$, $n = 3459$) and the OL (supermicrometer $88\% \pm 2\%$, $n = 516$; submicrometer $66\% \pm 1\%$, $n = 1912$) and IF4 experiments (supermicrometer $97.6\% \pm 0.6\%$, $n = 651$; submicrometer $65.8\% \pm 0.8\%$, $n = 2355$). As discussed in Section 3.2, the SSA size distribution for the IF+A experiment was also similar to that of IF1 and IF3 (though the mode diameter was slightly smaller). The ice algal aggregates added to the IF water for this experiment resulted in lower salinity and larger concentrations of chlorophyll *a*, POC, PN, and greater abundances of eutrophic pico-nanoplankton and heterotrophic nanoplankton compared to the four IF experiments. However, these differences did not translate into a greater number fraction of organic particles in the generated SSA. This result is in agreement with our recent study that showed little change in the number fractions of organic and sea salt particles ($0.12\text{--}7.05\text{ }\mu\text{m } d_{pa}$) generated from Gulf of Maine seawater when the DOC concentration was increased from $95\text{ }\mu\text{M}$ to $400\text{ }\mu\text{M}$ (Mirrielees et al., 2022). Other studies have shown a direct relationship (O'Dowd et al., 2004), or a lack of relationship (Quinn et al., 2014), between biological activity and the organic aerosol mass fraction, or a complex relationship in which community dynamics impact the composition of organics in aerosol particles (Wang et al., 2015). The complex relationship between SSA composition and the concentration of DOC

and chlorophyll *a*, as well as the abundance of bacteria and phytoplankton, must be elucidated through further study.

The distribution of particle types generated from MP water was similar to that from the IF1, IF2, IF4, and OL experiments (**Figure 5**), despite large differences in the salinity, chlorophyll *a*, DOC (**Figure 2**), the composition of the microbial community (**Figure 3**), and the SSA size distribution (**Figure 4**) between these experiments. Recently, Zeppenfeld et al. (2023) measured aerosol-relevant marine carbohydrates in various Arctic Ocean water samples and noted the variability across melt ponds. Overall, future studies on the composition and potential generation mechanism of melt pond aerosol are critical to assess this potential High Arctic aerosol source.

3.4. Composition of organic compounds in SSA

Raman spectral analysis was used to classify the organic material in 313 individual SSA particles collected during the MART experiments using MOUDI stages corresponding to 0.32–0.56 μm d_a and 1.0–1.8 μm d_a (i.e., submicrometer and supermicrometer particles, respectively). These Raman spectra were classified as carbohydrates, long-chain fatty acids ($>C_{10}$), or organic “siliceous material,” using the approach developed by Cochran et al. (2017). These assignments are described in Text S2 and Tables S4, S5, and S6; inorganic spectra assignments are included in Table S7. Representative Raman spectra of each type are shown in **Figure 7a**. Average Raman spectra for submicrometer and supermicrometer particles collected during each MART experiment are shown in **Figure S6**. Neither amino acids nor proteins were identified among the collected Raman spectra.

Carbohydrates accounted for the majority of the assigned single-particle Raman spectra (225 out of 313 particles), as shown in **Figures 7b** and S7. Each of these spectra was matched with the CARB (carbohydrate) library spectrum that was collected from SSA in a previous study (Cochran et al., 2017). For most of the experiments and SSA particle size ranges, carbohydrates accounted for 81–100%, by number, of the single-particle Raman spectra. The outliers were submicrometer particles generated during IF2 ($8\% \pm 8\%$ carbohydrates, $n = 12$), submicrometer particles generated during IF+A ($50\% \pm 10\%$ carbohydrates, $n = 15$), and both submicrometer and supermicrometer particles generated during MP (0% carbohydrates for both particle size ranges).

The carbohydrate Raman spectrum of this study is similar to Raman spectra collected from ambient SSA particles in the summertime Antarctic air (Eom et al., 2016), as well as SSA generated in mesocosm tanks using seawater collected from the California coast and the Gulf of Maine (Mirrielees et al., 2022). The observation of this Raman spectrum in ambient and laboratory-generated SSA from diverse locations, and during different years, indicates that these carbohydrates are widely distributed throughout the ocean’s surface. Most (70–95%) of the DOM in the ocean is refractory, with a lifetime of approximately 16,000 years (Davis and Benner, 2005; Hansell, 2013). A smaller fraction (6–30%) is semi-labile, with a lifetime of approximately 1.5 years and only a small fraction

(0.03–5%) that is considered to be labile, or freshly generated, with a lifetime of hours or days (Davis and Benner, 2005; Hansell, 2013). Refractory DOM can be transported from the ocean into the aerosol phase (Beaupré et al., 2019; Lawler et al., 2020) via bubble bursting at the surface of the ocean, which is facilitated by the presence of surface-active organic matter (Kieber et al., 2016). Previous studies suggest that the organic component of SSA is dominated by a background pool of DOM rather than fresh organic compounds produced by the local biological community (Quinn et al., 2014; Bates et al., 2020; Santander et al., 2022). The widespread observance of carbohydrates in SSA may indicate that this “carbohydrate” Raman spectrum is representative of refractory DOM. Polysaccharides (Hawkins and Russell, 2010; Chang et al., 2011; Gao et al., 2012; Fu et al., 2013; Leck et al., 2013; Choi et al., 2019) are commonly identified organic components of Arctic SSA. Additionally, carboxyl-rich alicyclic molecules have been identified as a major component of refractory DOM (Hertkorn et al., 2006). While no Raman spectrum of carboxyl-rich alicyclic molecules has been published at this time, these molecules would be expected to contain C-C, C-O, C=O, C-H, and O-H bonds, which were detected in the carbohydrate Raman spectrum in our study (Table S4).

Long-chain fatty acids (LCFA, mostly C_{12} – C_{22}) were identified in SSA during several of the experiments (**Figures 7b** and S7). LCFA are ubiquitous in marine environments and have previously been identified in Arctic sea ice (Kohlbach et al., 2016; Kohlbach et al., 2020) and SSA (Fu et al., 2013; Kirpes et al., 2019). LCFA are known to be produced by Arctic diatoms (Falk-Petersen et al., 1998; Henderson et al., 1998) and dinoflagellates (Falk-Petersen et al., 1998). LCFA were identified in 40 of the 313 individual particles analyzed. The number fraction of submicrometer particles containing fatty acids ($\leq 10\%$) was generally similar to the number fraction of supermicrometer particles containing fatty acids ($\leq 9\%$) for the MIZ, NP, IF1–4, IF+A, and OL experiments. This similarity contrasts with a previous study in which larger number fractions of individual particles containing fatty acids were observed in submicrometer SSA compared to supermicrometer SSA (Cochran et al., 2017). Larger number fractions of individual particles containing LCFA were observed during the MP experiment, for which LCFA accounted for $96\% \pm 4\%$ of submicrometer SSA ($n = 28$) and $25\% \pm 8\%$ of supermicrometer SSA ($n = 28$). A recent lab study found that SSA concentration is suppressed by fatty acids and enhanced by dissolved saccharides (Xu et al., 2024). Together with the lower salinity of the MP water, the relatively low total aerosol particle concentration measured for the MP experiment compared to the other MART experiments is consistent with this recent finding.

The relatively low fractions of LCFA in eight of the MART experiments, compared with the larger fractions of LCFA in the MP experiment, may be due to the lability of fatty acids (Mochida et al., 2002), which are produced by phytoplankton and consumed readily by heterotrophic bacteria (Wang et al., 2015; Cochran et al., 2017). In

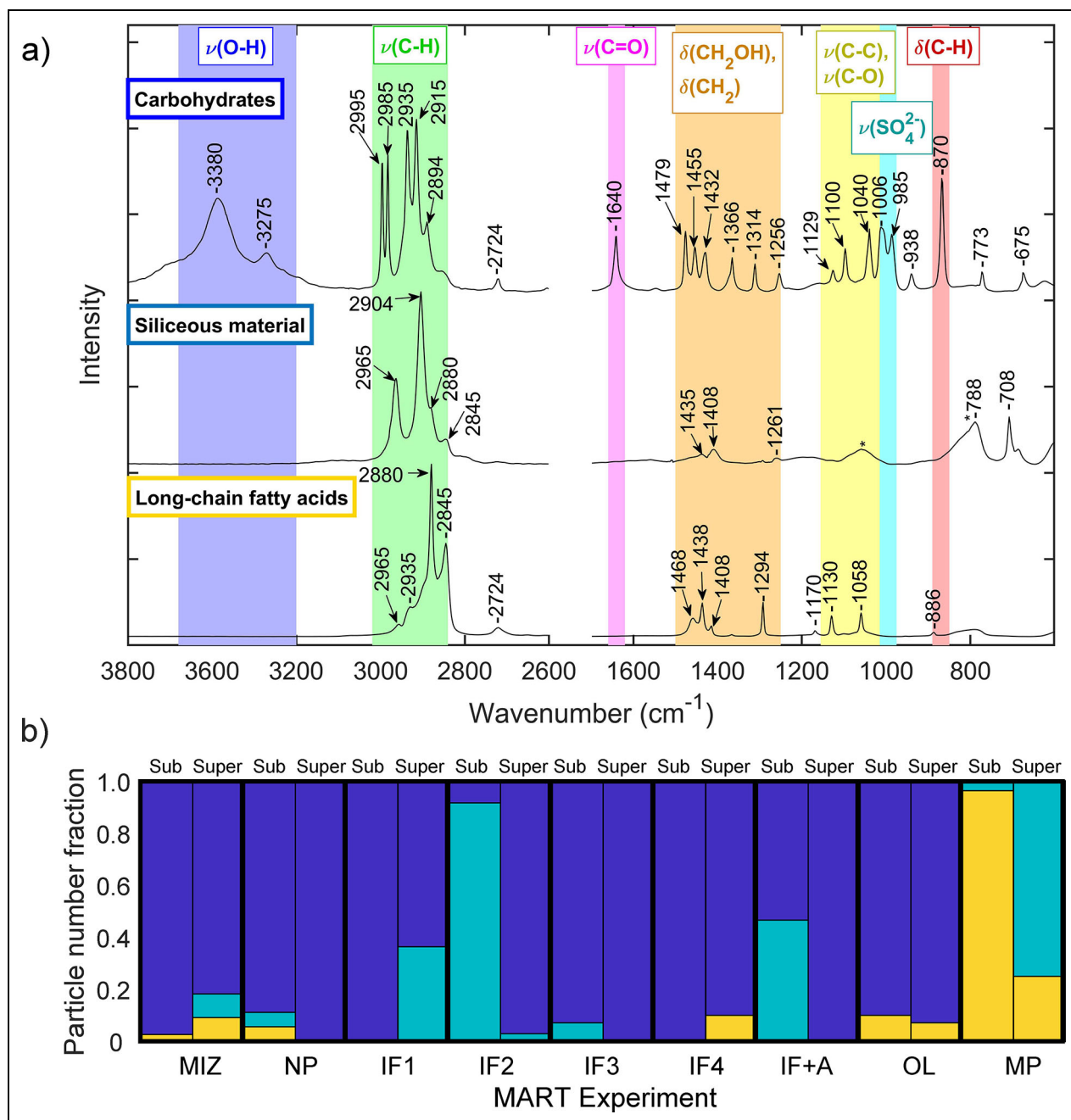


Figure 7. Organic composition of individual aerosol particles. (a) Raman spectra of three representative individual particles with organic compounds identified as carbohydrates, organic siliceous material (which contains organic functional groups), and long-chain fatty acids. These spectra were obtained from a supermicrometer IF4 particle, a supermicrometer MP particle, and a submicrometer MP particle, respectively. (b) Number fractions of individual submicrometer (Sub) and supermicrometer (Super) particles corresponding to each observed organic composition type.

contrast with the seawater locations from which the MIZ, NP, IF1–4, IF+A, and OL experimental waters were collected, melt ponds are short-lived ecosystems (Sørensen et al., 2017). The melt pond in the current study would have formed recently due to melting of snow on the surface of the ice floe. The relatively “fresh” MP water may have contained a greater concentration of LCFA (compared to carbohydrates) due to production of labile fatty acids by autotrophic species, and a lack of an established heterotrophic community that would

normally consume them. The concentrations of dissolved and particulate carbohydrates increase with melt pond age (Zeppenfeld et al., 2023), which further suggests that the MP water was collected from a relatively young melt pond. The lack of carbohydrates in the MP SSA, and their prevalence throughout the other eight MART experiments in which surface water was sampled from the relatively “older” Arctic seawater, provides further support for the carbohydrate Raman spectrum representing refractory DOM.

Overall, 48 of the 313 particles analyzed using Raman microspectroscopy were identified as organic “siliceous material.” The individual particle Raman spectrum characterized as organic siliceous material in **Figure 7a** is nearly identical to the organic siliceous material identified in SSA generated from coastal California seawater (Cochran et al., 2017). This siliceous material Raman spectrum is nearly identical to the Raman spectrum of polydimethylsiloxane (Kammer et al., 2010; Kim et al., 2017), a polymer with many applications (Ariati et al., 2021; Ribeiro and Lima, 2022). Note that Raman spectra collected from diatoms (Kammer et al., 2010; Pinzaru et al., 2016; R uger et al., 2016; De Tommasi et al., 2018; Ahmmed et al., 2021; Akse et al., 2021) differ from the siliceous material in the current study. In particular, modes associated with SiO_4 symmetric stretching ($768\text{--}850\text{ cm}^{-1}$; De Tommasi et al., 2018; Akse et al., 2021), Si-OH stretching ($900\text{--}1050\text{ cm}^{-1}$; De Tommasi et al., 2018; Akse et al., 2021), carotenoids (1014 cm^{-1} , 1162 cm^{-1} , 1180 cm^{-1} , 1528 cm^{-1} ; Pinzaru et al., 2016; R uger et al., 2016), and chlorophyll *a* (986 cm^{-1} , 1224 cm^{-1} , 1328 cm^{-1} ; R uger et al., 2016) were not detected in the siliceous material. The origin of the siliceous material in the particles generated from the surface waters is unknown. Number fractions of siliceous material (**Figures 7b** and S7) were elevated in certain experiments with no discernible patterns, accounting for $40\% \pm 10\%$ ($n = 11$) of the supermicrometer IF1 SSA particles, $92\% \pm 8\%$ ($n = 12$) of the submicrometer IF2 SSA particles, $75\% \pm 8\%$ ($n = 28$) of the supermicrometer MP SSA particles in the range $1.0\text{--}1.8\text{ }\mu\text{m } d_a$, and $50\% \pm 10\%$ ($n = 15$) of the submicrometer IF+A SSA particles, with fractions of 0–9% observed in all other samples.

Note that amino acids were not detected in any of the analyzed particles. Amino acids have been detected previously in aerosol particles, including from sea spray, in the High Arctic (Scalabrin et al., 2012; Fu et al., 2015), and elsewhere in the Arctic (Hawkins and Russell, 2010; Logvinova et al., 2016; Kirpes et al., 2019). Previous studies have observed amino acid enrichment in SSA generated via plunging jet (Kuznetsova et al., 2005; Triesch et al., 2021) and in ambient SSA (van Pinxteren et al., 2023). However, other studies have found that MART-generated SSA may be depleted in amino acids (Decesari et al., 2020) or be characterized by a different amino acid signature (Santander et al., 2021) compared to the seawater from which it was generated. The experimental waters collected during the current study may have contained amino acids or proteins that were not transferred to the aerosol phase. Some of the generated particles may also have contained amino acids, but in such a small quantity that they could not be clearly identified from the collected Raman spectra.

3.5. Ice-nucleating particle measurements

We present in Figure S8 the size-resolved cumulative INP concentration spectra (INP concentration per volume of suspension, as a function of activation temperature) for the air in the headspace above the MART tank. Comparison of the INP spectra for the MART samples with those for the blanks reveals that there is no discernible difference between the two in the majority of the samples.

Hence, the INP spectra reported here represent upper limits to the INP concentrations; that is, the INP concentration was lower than the quoted limiting values. The one exception is the MP MART experiment, for which some weak measurable activity appears above the baseline in all size bins apart from the largest ($5.6\text{--}10\text{ }\mu\text{m } d_a$). Aerosol particles generated from the MP water were rich in aliphatic hydrocarbons (Section 3.4), which have been identified as being important for marine sources of INPs in wave tank experiments (Wang et al., 2015). Another study found that the concentration of free glucose correlated positively with the ice nucleation activity of bulk seawater and the sea surface microlayer (Zeppenfeld et al., 2019), which is inconsistent with the higher INP concentrations measured during the MP experiment (organics dominated by fatty acids) compared to the MIZ, NP, IF1–4, IF+A, and OL experiments (organics dominated by carbohydrates). However, the general result, particularly for the seawater MART experiments, is that the ice-nucleating activity of the aerosol generated in the MART was not strong enough to be above the background.

In order to compare the MART INP concentrations to the ambient INP concentrations from the whole air inlet during MOCCHA (Porter et al., 2022), we derived the INP concentration from the sample volume and wash volume (see Methods) and normalized to the median campaign ambient aerosol concentration (74 cm^{-3} ; Karlsson and Zieger, 2020) as the aerosol concentrations in the MART were greater than in the ambient atmosphere. The result is shown in **Figure 8**. If all aerosol particles in the Arctic boundary layer that we sampled via the whole air inlet were derived from local SSA production, then the maximum INP concentration we would expect from this source is represented by the normalized MART INP concentrations in **Figure 8**. Clear from this plot is that local SSA cannot account for the relatively high ice-nucleating activity of the aerosol observed on many days during the MOCCHA campaign when concentrations at -15°C sometimes were as high as 2 L^{-1} (Porter et al., 2022). However, the MP experimental water produced some INPs at around -20°C , and the total INP concentration (summed across the six size bins) is approximately 0.1 L^{-1} . This value, though still substantially lower than the observed atmospheric INP concentrations on many days, does indicate the need for further work in characterizing INPs produced from a range of high-latitude marine sources, including melt ponds.

Based on backward air mass trajectory analysis, Porter et al. (2022) concluded that the ambient samples with high ice-nucleating activities corresponded to air masses traveling from near the Russian coast. In contrast, the ice-nucleating activities of ambient samples were much lower on days when the air circulated around the pack ice. These pack ice trajectory INP spectra from Porter et al. (2022) are consistent with the MART results in **Figure 8**. Bearing in mind that the MART INP concentrations are upper limits, local SSA may have been an important source of INPs on these days.

Alpert et al. (2022) suggest that all SSA can serve as INPs, regardless of whether they are derived from seawater

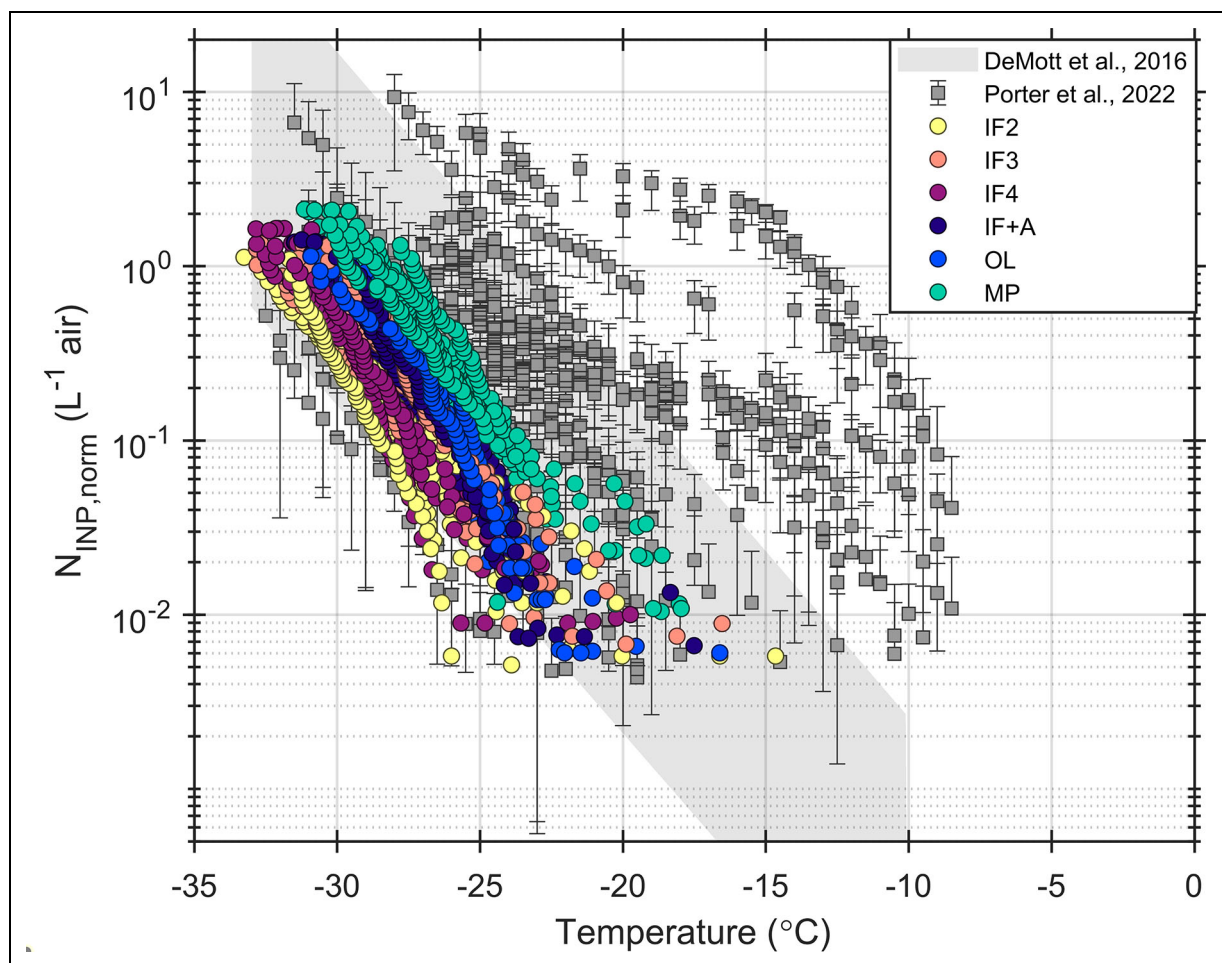


Figure 8. Ice-nucleating particles (INPs) derived from the MART experiments. Upper limits to the INP concentrations derived from the marine aerosol reference tank (MART) experiments compared to atmospheric INP concentrations from the same cruise (Porter et al., 2022). The range of “typical marine” INP concentrations reported by DeMott et al. (2016), as shown in McCluskey et al. (2018), have also been included for comparison. The MART INP concentrations are quoted as upper limits because in most cases no enhanced freezing was observed above the pure water handling blanks (Figure S7). The MART INP concentrations were normalized to the median campaign ambient aerosol concentration (74 cm^{-3} for particles $10\text{--}921 \text{ nm } d_m$; Karlsson and Zieger, 2020) in order to compare the INP concentrations with ambient values.

with a high or low level of microbial activity (within uncertainty). Some previous authors have suggested open leads, melt ponds, and the pack ice as sources of INPs (Hartmann et al., 2020; Creamean et al., 2022), and previous work has shown that open leads, melt ponds, and seawater harbor biological ice-nucleating entities (Wilson et al., 2015; DeMott et al., 2016; Irish et al., 2017; Zeppenfeld et al., 2019). The transfer of this material into the atmosphere through SSA production typically defines a relatively low background INP concentration (Vergara-Temprado et al., 2017; Ickes et al., 2020), ranging from 10^{-3} L^{-1} to 0.1 L^{-1} at -20°C (DeMott et al., 2016; McCluskey et al., 2018). INP concentrations measured in our MART experimental waters (Figure 8) are consistent with these previously reported low concentrations. Hence, in previous campaigns (Hartmann et al., 2020; Creamean et al., 2022), the dominant sources of INPs may have been local marine sources, rather than sporadic input from further afield. The concept of SSA providing a steady background

INP concentration, with periods of days where more distant sources dominate, is also relevant for the Southern Ocean where sea spray sources are thought to control the very low INP concentrations on most days, with sporadic dust input from terrestrial locations dominating on some days (Vergara-Temprado et al., 2017).

4. Summary and conclusions

As the Arctic continues to warm nearly four times as quickly as the rest of the Earth (Rantanen et al., 2022), elucidating the factors that control the concentration and composition of SSA from open water, leads, and potentially melt ponds in the Arctic is important. Ten SSA generation experiments were carried out using a MART with locally collected water during the MOCCHA expedition to the High Arctic pack ice during August–September 2018. Experimental waters were collected from various sites, including the MIZ, a human-made sea ice hole near the North Pole, leads next to an ice floe, and a melt pond.

The connections between the chemical and biological characteristics of the surface experimental waters and the physical and chemical properties of the SSA generated are complex. No statistically significant correlations were found between the concentrations of chlorophyll *a*, POC, or PN or the abundances of heterotrophic nanoplankton or bacteria and total aerosol particle concentration or submicrometer mode diameter. Yet, both total aerosol particle concentration and submicrometer mode diameter correlated positively with DON concentration. An increased concentration of dissolved organic compounds in seawater has previously been shown to result in increased SSA concentration (Lv et al., 2020). The lack of a clear relationship between the biological measurements and SSA concentration may stem from the complex nature of microbial communities and their varying levels of extracellular release of DOM (Vernet et al., 2021) which also impact SSA chemical composition. The filtered seawater experiment produced a similar SSA mode diameter but lower concentration compared to unfiltered seawater, also pointing to the role of particulate matter in the water in contributing to SSA production. The lowest total aerosol particle concentration and the smallest mode diameter were observed for the melt pond water aerosol, consistent with the lowest water salinity.

Sea salt aerosol constituted 44–95% of individual submicrometer and 68–100% of supermicrometer particles, by number, generated across the experiments. As evidenced by visible organic coatings, carbon was detected in >80%, by number, of these sea salt particles. Greater carbon enrichment, as well as divalent cation enrichment, was measured in submicrometer sea salt particles ($C/Na = 0.27\text{--}0.41$) compared to supermicrometer sea salt particles ($C/Na = 0.06\text{--}0.14$), in agreement with previous measurements of exopolymer gels coating Arctic sea salt aerosol particles when sea ice was nearby (Facchini et al., 2008; Kirpes et al., 2019). The measured C/Na ratios are not correlated with the concentrations of chlorophyll *a*, DOC, DON, POC, or PN or with the abundances of eukaryotic pico-nanoplankton, heterotrophic nanoplankton, or bacteria, which suggests that the enrichment of carbon in sea salt particles is influenced by additional factors beyond the quantity of carbon and nitrogen in the seawater, or the abundance of cells capable of producing organic exudates. In agreement with previous studies (Ault et al., 2013b; Prather et al., 2013; Kirpes et al., 2018), the majority of organic (non-sea salt) particles produced by sea spray fell within the submicrometer range. Carbohydrates were the dominant organic compound class identified in the individual SSA particles in all but the MP experiment, when the submicrometer particles were purely long-chain fatty acids and the supermicrometer particles were dominated by siliceous material. The prevalence of carbohydrates in seawater compared to the relatively “young” melt pond water suggests that the SSA generated from the experimental seawaters contained refractory DOM, which constitutes the majority of DOM in the ocean (Davis and Benner, 2005; Hansell, 2013).

As the Arctic warms, SSA production from leads in the Arctic Ocean is expected to increase as older, thicker sea ice is replaced by younger, thinner ice prone to fracturing (Richter-Menge and Farrell, 2013). The period of open water SSA production in the Arctic is lengthening as sea ice melt starts earlier in the spring (Stroeve et al., 2012) and freeze-up moves later in the fall (Serreze and Stroeve, 2015). Further, the local production of SSA in the Arctic has been observed year-round (May et al., 2016b). Clear from this study and others is the complex dependence of SSA concentration and composition on sea ice algae, phytoplankton, and other microbiota and the need for more studies to further investigate the details of these connections, especially given the logistical field limitations of the current work. This need is particularly important given increasing biological primary production and earlier growing seasons with declining Arctic sea ice (Tedesco et al., 2019; Lannuzel et al., 2020). SSA concentrations and composition are important for climate feedbacks, including cloud formation and properties (Quinn et al., 2015; Abbatt et al., 2019; Russell et al., 2023). Quantification of the ice-nucleating activity of the generated SSA in this study showed that locally produced SSA may define the High Arctic background INP population (Porter et al., 2022). Finally, our data suggest that melt ponds might provide a source of more active INP than seawater, which may be due to the greater fraction of long-chain fatty acids in aerosol particles generated from the melt pond water compared to the experimental seawaters. Clearly more research is needed to understand how changes in the biogeochemical properties of the Arctic surface are controlling SSA concentration, composition, and climate feedbacks.

Data accessibility statement

The 16S DNA sequences can be found in the NCBI.NLM.NIH BioProject database (<http://www.ncbi.nlm.nih.gov/bioproject/1084073>). The Arctic Ocean expedition cruise track data can be found in the Bolin database at <https://bolin.su.se/data/oden-ao-2018-expedition-1>. The surface water measurement data, 16S/18S DNA distribution data, aerosol size distribution data, particle number type distribution data, SSA mole ratio data, representative Raman spectra for carbohydrates, siliceous material, and long-chain fatty acids, and organic component distribution data can be found at the NSF Arctic Data Center at <https://arcticdata.io/catalog/view/doi%3A10.18739%2FA2QZ22J9F>. The ice-nucleating particle data from the MART experiments are available via the Bolin database at <https://doi.org/10.17043/oden-ao-2018-mart-aerosol-inp-1>.

Supplemental files

The supplemental files for this article can be found as follows:

Text S1. Individual SSA particle elemental ratios.

Text S2. Analysis of Raman spectra collected from individual SSA particles.

Table S1. Eukaryotic plankton community composition.

Table S2. Eukaryotic plankton diversity.

Table S3. Prokaryotic plankton community composition.

Table S4. Carbohydrate assignments of individual sea salt particles.

Table S5. Fatty acids assignments of individual sea salt particles.

Table S6. Siliceous assignments of individual sea salt particles.

Table S7. Inorganic chemical species assignments of individual sea salt particles.

Figure S1. Marine aerosol reference tank (MART).

Figure S2. Number and size of aerosol particles analyzed by CCSEM-EDX per MART experiment.

Figure S3. Experimental aerosol size distributions.

Figure S4. Sea spray aerosol particles from North Pole MART experiment.

Figure S5. Experimental aerosol molar ratios.

Figure S6. Experimental aerosol Raman spectra.

Figure S7. Experimental aerosol chemical composition.

Figure S8. Experimental ice nucleating particle concentrations.

Acknowledgments

We are indebted to Carlton D. Rauschenberg for cruise organization, sample acquisition, and overall field work coordination (Bigelow Laboratory for Ocean Sciences). We thank Allison Remenapp (Villanova University) for field work and acquisition of samples and data. Yao Xiao (University of Michigan) contributed to Raman data collection and analysis. We thank Vicki Grassian (University of California, San Diego) for providing the Raman library of standard organic compounds (Cochran et al., 2017). CCSEM-EDX analyses were performed at the Environmental Molecular Sciences Laboratory (EMSL), a national scientific user facility located at the Pacific Northwest National Laboratory (PNNL) and sponsored by the Office of Biological and Environmental Research of the U.S. Department of Energy. We thank the Hansell Laboratory (University of Miami) for measurements of DOC and DON, the Integrated Microbiome Resource (Dalhousie University) for the DNA analysis, and the Center for Aquatic Cytometry (Bigelow Laboratory for Ocean Sciences) for the flow cytometry analysis. We thank the Swedish Polar Research Secretariat and the crew of the I/B *Oden* for logistical support.

Funding

This work was supported by the National Science Foundation (OPP-1724585, 1724651, and 1724642). A portion of this research was performed on a project award 60327 from the Pacific Northwest National Laboratory Environmental Molecular Sciences Laboratory, a DOE Office of Science User Facility sponsored by the Biological and Environmental Research program under Contract No. DE-AC05-76RL01830. The INP measurements were supported by the European Research Council (ERC, Marinelce 648661). Lastly, we thank the University of Michigan and the Department of Chemistry for additional support.

Competing interests

The contact authors have declared that none of the authors has any competing interests.

Author contributions

Contributed to conception and design: PAM, KAP, AMG, APA.

Contributed to acquisition of samples and data: RMK, PAM, GCEP.

Contributed to analysis of samples and/or data: EJC, SC, RMK,>NNL, JAM, GCEP.

Contributed to analysis and interpretation of data: JAM, EJC, RMK, BJM, PAM, KAP, APA, VB, AMG.

Drafted and/or revised the article: JAM, PAM, KAP, BJM, APA, EJC, VB, AMG, SC,>NNL, RMK, GCEP.

Approved the submitted version for publication: All coauthors.

References

- Abbatt, JPD, Leaitch, WR, Aliabadi, AA, Bertram, AK, Blanchet, J-P, Boivin-Rioux, A, Bozem, H, Burkart, J, Chang, RYW, Charette, J, Chaubey, JP, Christensen, RJ, Cirisan, A, Collins, DB, Croft, B, Dionne, J, Evans, GJ, Fletcher, CG, Galí, M, Ghahreman, R, Girard, E, Gong, W, Gosselin, M, Gourdal, M, Hanna, SJ, Hayashida, H, Herber, AB, Hesaraki, S, Hoor, P, Huang, L, Hussherr, R, Irish, VE, Keita, SA, Kodros, JK, Köllner, F, Kolonjari, F, Kunkel, D, Ladino, LA, Law, K, Levasseur, M, Libois, Q, Liggio, J, Lizotte, M, Macdonald, KM, Mahmood, R, Martin, RV, Mason, RH, Miller, LA, Moravek, A, Mortenson, E, Mungall, EL, Murphy, JG, Namazi, M, Norman, A-L, O'Neill, NT, Pierce, JR, Russell, LM, Schneider, J, Schulz, H, Sharma, S, Si, M, Staebler, RM, Steiner, NS, Thomas, JL, von Salzen, K, Wentzell, JJB, Willis, MD, Wentworth, GR, Xu, J-W, Yakobi-Hancock, JD. 2019. Overview paper: New insights into aerosol and climate in the Arctic. *Atmospheric Chemistry and Physics* **19**: 2527–2560. DOI: <https://doi.org/10.5194/acp-19-2527-2019>.
- Ahmed, R, Prowse, T, Dibike, Y, Bonsal, B, O'Neil, H. 2020. Recent trends in freshwater influx to the Arctic Ocean from four major Arctic-draining rivers. *Water* **12**: 1189. DOI: <https://doi.org/10.3390/w12041189>.
- Ahmed, F, Fraser-Miller, SJ, Garagoda Arachchige, PS, Schallenberg, M, Novis, P, Gordon, KC. 2021. Lake snow caused by the invasive diatom *Lindavia intermedia* can be discriminated from different sites and from other algae using vibrational spectroscopy. *Journal of Raman Spectroscopy* **52**: 2597–2608. DOI: <https://doi.org/10.1002/jrs.6161>.
- Akse, SP, Das, G, Agustí, S, Pichevin, L, Polerecky, L, Middelburg, JJ. 2021. Imaging of organic signals in individual fossil diatom frustules with nanoSIMS and Raman spectroscopy. *Marine Chemistry* **228**: 103906. DOI: <https://doi.org/10.1016/j.marchem.2020.103906>.

- Alpert, PA, Kilhau, WP, Bothe, DW, Radway, JC, Aller, JY, Knopf, DA.** 2015. The influence of marine microbial activities on aerosol production: A laboratory mesocosm study. *Journal of Geophysical Research: Atmospheres* **120**: 8841–8860. DOI: <https://doi.org/10.1002/2015jd023469>.
- Alpert, PA, Kilhau, WP, O'Brien, RE, Moffet, RC, Gilles, MK, Wang, B, Laskin, A, Aller, JY, Knopf, DA.** 2022. Ice-nucleating agents in sea spray aerosol identified and quantified with a holistic multimodal freezing model. *Science Advances* **8**: eabq6842. DOI: <https://doi.org/10.1126/sciadv.abq6842>.
- Ardyna, M, Babin, M, Gosselin, M, Devred, E, Bélanger, S, Matsuoka, A, Tremblay, J-É.** 2013. Parameterization of vertical chlorophyll *a* in the Arctic Ocean: Impact of the subsurface chlorophyll maximum on regional, seasonal, and annual primary production estimates. *Biogeosciences* **10**: 4383–4404. DOI: <https://doi.org/10.5194/bg-10-4383-2013>.
- Ariati, R, Sales, F, Souza, A, Lima, RA, Ribeiro, J.** 2021. Polydimethylsiloxane composites characterization and its applications: A review. *Polymers* **13**: 4258. DOI: <https://doi.org/10.3390/polym13234258>.
- Assmy, P, Ehn, JK, Fernández-Méndez, M, Hop, H, Katlein, C, Sundfjord, A, Bluhm, K, Daase, M, Engel, A, Fransson, A, Granskog, MA, Hudson, SR, Kristiansen, S, Nicolaus, M, Peeken, I, Renner, AHH, Spreen, G, Tatarek, A, Wiktor, J.** 2013. Floating ice-algal aggregates below melting Arctic sea ice. *PLoS One* **8**: e76599. DOI: <https://doi.org/10.1371/journal.pone.0076599>.
- Ault, AP, Guasco, TL, Ryder, OS, Baltrusaitis, J, Cuadra-Rodriguez, LA, Collins, DB, Ruppel, MJ, Bertram, TH, Prather, KA, Grassian, VH.** 2013a. Inside versus outside: Ion redistribution in nitric acid reacted sea spray aerosol particles as determined by single particle analysis. *Journal of the American Chemical Society* **135**: 14528–14531. DOI: <https://doi.org/10.1021/ja407117x>.
- Ault, AP, Moffet, RC, Baltrusaitis, J, Collins, DB, Ruppel, MJ, Cuadra-Rodriguez, LA, Zhao, D, Guasco, TL, Ebben, CJ, Geiger, FM, Bertram, TH, Prather, KA, Grassian, VH.** 2013b. Size-dependent changes in sea spray aerosol composition and properties with different seawater conditions. *Environmental Science & Technology* **47**: 5603–5612. DOI: <https://doi.org/10.1021/es400416g>.
- Ault, AP, Peters, TM, Sawvel, EJ, Casuccio, GS, Willis, RD, Norris, GA, Grassian, VH.** 2012. Single-particle SEM-EDX analysis of iron-containing coarse particulate matter in an urban environment: Sources and distribution of iron within Cleveland, Ohio. *Environmental Science & Technology* **46**: 4331–4339. DOI: <https://doi.org/10.1021/es204006k>.
- Barr, SL, Wyld, B, McQuaid, JB, Neely, RR III, Murray, BJ.** 2023. Southern Alaska as a source of atmospheric mineral dust and ice-nucleating particles. *Science Advances* **9**: eadg3708. DOI: <https://doi.org/10.1126/sciadv.adg3708>.
- Bates, TS, Quinn, PK, Coffman, DJ, Johnson, JE, Upchurch, L, Saliba, G, Lewis, S, Graff, J, Russell, LM, Behrenfeld, MJ.** 2020. Variability in marine plankton ecosystems are not observed in freshly emitted sea spray aerosol over the North Atlantic Ocean. *Geophysical Research Letters* **47**: e2019GL085938. DOI: <https://doi.org/10.1029/2019GL085938>.
- Beaupré, SR, Kieber, DJ, Keene, WC, Long, MS, Maben, JR, Lu, X, Zhu, Y, Frossard, AA, Kinsey, JD, Duplessis, P, Chang, RY-W, Bisgrove, J.** 2019. Oceanic efflux of ancient marine dissolved organic carbon in primary marine aerosol. *Science Advances* **5**: eaax6535. DOI: <https://doi.org/10.1126/sciadv.aax6535>.
- Bertram, TH, Cochran, RE, Grassian, VH, Stone, EA.** 2018. Sea spray aerosol chemical composition: Elemental and molecular mimics for laboratory studies of heterogeneous and multiphase reactions. *Chemical Society Reviews* **47**: 2374–2400. DOI: <https://doi.org/10.1039/c7cs00008a>.
- Bigg, EK, Leck, C.** 2001. Cloud-active particles over the central Arctic Ocean. *Journal of Geophysical Research: Atmospheres* **106**: 32155–32166. DOI: <https://doi.org/10.1029/1999JD901152>.
- Bigg, EK, Leck, C.** 2008. The composition of fragments of bubbles bursting at the ocean surface. *Journal of Geophysical Research: Atmospheres* **113**: 1–7. DOI: <https://doi.org/10.1029/2007JD009078>.
- Brooks, IM, Yelland, MJ, Upstill-Goddard, RC, Nightingale, PD, Archer, S, d'Asaro, E, Beale, R, Beatty, C, Blomquist, B, Bloom, AA, Brooks, BJ, Cluderay, J, Coles, D, Dacey, J, DeGrandpre, M, Dixon, J, Drennan, WM, Gabriele, J, Goldson, L, Hardman-Mountford, N, Hill, MK, Horn, M, Hsueh, P-C, Huebert, B, de Leeuw, G, Leighton, TG, Liddicoat, M, Lingard, JJN, McNeil, C, McQuaid, JB, Moat, BI, Moore, G, Neill, C, Norris, SJ, O'Doherty, S, Pascal, RW, Prytherch, J, Rebozo, M, Sahlee, E, Salter, M, Schuster, U, Skjelvan, I, Slagter, H, Smith, MH, Smith, PD, Srokosz, M, Stephens, JA, Taylor, PK, Telszewski, M, Walsh, R, Ward, B, Woolf, DK, Young, D, Zemmeling, H.** 2009. Physical exchanges at the air–sea interface: UK–SOLAS field measurements. *Bulletin American Meteorological Society* **90**: 629–644. DOI: <https://doi.org/10.1175/2008BAMS2578.1>.
- Browse, J, Carslaw, KS, Mann, GW, Birch, CE, Arnold, SR, Leck, C.** 2014. The complex response of Arctic aerosol to sea-ice retreat. *Atmospheric Chemistry and Physics* **14**: 7543–7557. DOI: <https://doi.org/10.5194/acp-14-7543-2014>.
- Brussaard, CPD.** 2004. Optimization of procedures for counting viruses by flow cytometry. *Applied and Environmental Microbiology* **70**: 1506–1513. DOI: <https://doi.org/10.1128/AEM.70.3.1506-1513.2004>.
- Bussmann, I, Kattner, G.** 2000. Distribution of dissolved organic carbon in the central Arctic Ocean: The influence of physical and biological properties.

- Journal of Marine Systems* **27**: 209–219. DOI: [https://doi.org/10.1016/S0924-7963\(00\)00068-3](https://doi.org/10.1016/S0924-7963(00)00068-3).
- Chang, RY-W, Leck, C, Graus, M, Müller, M, Paatero, J, Burkhardt, JF, Stohl, A, Orr, LH, Hayden, K, Li, S-M, Hansel, A, Tjernström, M, Leaitch, WR, Abbatt, JPD.** 2011. Aerosol composition and sources in the central Arctic Ocean during ASCOS. *Atmospheric Chemistry and Physics* **11**: 10619–10636. DOI: <https://doi.org/10.5194/acp-11-10619-2011>.
- Chen, Q, Mirrielees, JA, Thanekar, S, Loeb, NA, Kirpes, RM, Upchurch, LM, Barget, AJ, Lata, NN, Raso, ARW, McNamara, SM, China, S, Quinn, PK, Ault, AP, Kennedy, A, Shepson, PB, Fuentes, JD, Pratt, KA.** 2022. Atmospheric particle abundance and sea salt aerosol observations in the springtime Arctic: A focus on blowing snow and leads. *Atmospheric Chemistry and Physics* **22**: 15263–15285. DOI: <https://doi.org/10.5194/acp-22-15263-2022>.
- Chi, JW, Li, WJ, Zhang, DZ, Zhang, JC, Lin, YT, Shen, XJ, Sun, JY, Chen, JM, Zhang, XY, Zhang, YM, Wang, WX.** 2015. Sea salt aerosols as a reactive surface for inorganic and organic acidic gases in the Arctic troposphere. *Atmospheric Chemistry and Physics* **15**: 11341–11353. DOI: <https://doi.org/10.5194/acp-15-11341-2015>.
- Chin, W-C, Orellana, MV, Verdugo, P.** 1998. Spontaneous assembly of marine dissolved organic matter into polymer gels. *Nature* **391**: 568–572. DOI: <https://doi.org/10.1038/35345>.
- Choi, JH, Jang, E, Yoon, YJ, Park, JY, Kim, T-W, Becagli, S, Caiazzo, L, Cappelletti, D, Krejci, R, Eleftheriadis, K, Park, K-T, Jang, KS.** 2019. Influence of biogenic organics on the chemical composition of Arctic aerosols. *Global Biogeochemical Cycles* **33**: 1238–1250. DOI: <https://doi.org/10.1029/2019GB006226>.
- Christaki, U, Courties, C, Massana, R, Catala, P, Lebaron, P, Gasol, JM, Zubkov, MV.** 2011. Optimized routine flow cytometric enumeration of heterotrophic flagellates using SYBR Green I. *Limnology and Oceanography: Methods* **9**: 329–339. DOI: <https://doi.org/10.4319/lom.2011.9.329>.
- Christiansen, S, Ickes, L, Bulatovic, I, Leck, C, Murray, BJ, Bertram, AK, Wagner, R, Gorokhova, E, Salter, ME, Ekman, AML, Bilde, M.** 2020. Influence of Arctic microlayers and algal cultures on sea spray hygroscopicity and the possible implications for mixed-phase clouds. *Journal of Geophysical Research: Atmospheres* **125**: e2020JD032808. DOI: <https://doi.org/10.1029/2020JD032808>.
- Christiansen, S, Salter, ME, Gorokhova, E, Nguyen, QT, Bilde, M.** 2019. Sea spray aerosol formation: Laboratory results on the role of air entrainment, water temperature, and phytoplankton biomass. *Environmental Science & Technology* **53**: 13107–13116. DOI: <https://doi.org/10.1021/acs.est.9b04078>.
- Cochran, RE, Jayarathne, T, Stone, EA, Grassian, VH.** 2016. Selectivity across the interface: A test of surface activity in the composition of organic-enriched aerosols from bubble bursting. *The Journal of Physical Chemistry Letters* **7**: 1692–1696. DOI: <https://doi.org/10.1021/acs.jpcllett.6b00489>.
- Cochran, RE, Laskina, O, Trueblood, JV, Estillero, AD, Morris, HS, Jayarathne, T, Sultana, CM, Lee, C, Lin, P, Laskin, J, Laskin, A, Dowling, JA, Qin, Z, Cappa, CD, Bertram, TH, Tivanski, AV, Stone, EA, Prather, KA, Grassian, VH.** 2017. Molecular diversity of sea spray aerosol particles: Impact of ocean biology on particle composition and hygroscopicity. *Chem* **2**: 655–667. DOI: <https://doi.org/10.1016/j.chempr.2017.03.007>.
- Collins, DB, Zhao, DF, Ruppel, MJ, Laskina, O, Grandquist, JR, Modini, RL, Stokes, MD, Russell, LM, Bertram, TH, Grassian, VH, Deane, GB, Prather, KA.** 2014. Direct aerosol chemical composition measurements to evaluate the physicochemical differences between controlled sea spray aerosol generation schemes. *Atmospheric Measurement Techniques* **7**: 3667–3683. DOI: <https://doi.org/10.5194/amt-7-3667-2014>.
- Comeau, AM, Douglas, GM, Langille, MGI.** 2017. Microbiome helper: A custom and streamlined workflow for microbiome research. *mSystems* **2**. DOI: <https://doi.org/10.1128/msystems.00127-16>.
- Comeau, AM, Kwawukume, A.** 2023. Preparing multiplexed 16S/18S/ITS amplicons for the Illumina MiSeq. DOI: <https://doi.org/10.17504/protocols.io.4r3l277k3g1y/v1>. Available at <https://www.protocols.io/view/preparing-multiplexed-16s-18s-its-amplicons-for-th-ci2jugcn.pdf>.
- Comiso, JC.** 2002. A rapidly declining perennial sea ice cover in the Arctic. *Geophysical Research Letters* **29**: 17-1. DOI: <https://doi.org/10.1029/2002GL015650>.
- Cornwell, GC, Sultana, CM, Prank, M, Cochran, RE, Hill, TCJ, Schill, GP, DeMott, PJ, Mahowald, N, Prather, KA.** 2020. Ejection of dust from the ocean as a potential source of marine ice nucleating particles. *Journal of Geophysical Research: Atmospheres* **125**: e2020JD033073. DOI: <https://doi.org/10.1029/2020JD033073>.
- Craig, RL, Bondy, AL, Ault, AP.** 2017. Computer-controlled Raman microspectroscopy (CC-Raman): A method for the rapid characterization of individual atmospheric aerosol particles. *Aerosol Science and Technology* **51**: 1099–1112. DOI: <https://doi.org/10.1080/02786826.2017.1337268>.
- Creamean, JM, Barry, K, Hill, TCJ, Hume, C, DeMott, PJ, Shupe, MD, Dahlke, S, Willmes, S, Schmale, J, Beck, I, Hoppe, CJM, Fong, A, Chamberlain, E, Bowman, J, Scharien, R, Persson, O.** 2022. Annual cycle observations of aerosols capable of ice formation in central Arctic clouds. *Nature Communications* **13**: 3537. DOI: <https://doi.org/10.1038/s41467-022-31182-x>.
- Dall'Osto, M, Ovadnevaite, J, Paglione, M, Beddows, DC, Ceburnis, D, Cree, C, Cortés, P, Zamanillo, M, Nunes, SO, Pérez, GL, Ortega-Retuerta, E.** 2017. Antarctic sea ice region as a source of biogenic organic nitrogen in aerosols. *Scientific Reports* **7**:

6047. DOI: <https://doi.org/10.1038/s41598-017-06188-x>.
- Dall'Osto, M, Vaqué, D, Sotomayor-Garcia, A, Cabrera-Brufau, M, Estrada, M, Buchaca, T, Soler, M, Nunes, S, Zeppenfeld, S, van Pinxteren, M, Herrmann, H, Wex, H, Rinaldi, M, Paglione, M, Beddows, DCS, Harrison, RM, Berdalet, E.** 2022. Sea ice microbiota in the Antarctic Peninsula modulates cloud-relevant sea spray aerosol production. *Frontiers in Marine Science* **9**: 827061. DOI: <https://doi.org/10.3389/fmars.2022.827061>.
- Darby, DA, Myers, WB, Jakobsson, M, Rigor, I.** 2011. Modern dirty sea ice characteristics and sources: The role of anchor ice. *Journal of Geophysical Research: Oceans* **116**. DOI: <https://doi.org/10.1029/2010JC006675>.
- Darby, DA, Polyak, L, Jakobsson, M.** 2009. The 2005 HOTRAX Expedition to the Arctic Ocean. *Global and Planetary Change* **68**: 1–4. DOI: <https://doi.org/10.1016/j.gloplacha.2009.04.005>.
- Davis, J, Benner, R.** 2005. Seasonal trends in the abundance, composition and bioavailability of particulate and dissolved organic matter in the Chukchi/Beaufort Seas and western Canada Basin. *Deep Sea Research Part II: Topical Studies in Oceanography* **52**: 3396–3410. DOI: <https://doi.org/10.1016/j.dsr2.2005.09.006>.
- de Leeuw, G, Andreas, EL, Anguelova, MD, Fairall, CW, Lewis, ER, O'Dowd, C, Schulz, M, Schwartz, SE.** 2011. Production flux of sea spray aerosol. *Review of Geophysics* **49**: 1–5. DOI: <https://doi.org/10.1029/2010RG000349>.
- De Tommasi, E, Congestri, R, Dardano, P, De Luca, AC, Managò, S, Rea, I, De Stefano, M.** 2018. UV-shielding and wavelength conversion by centric diatom nanopatterned frustules. *Scientific Reports* **8**: 16285. DOI: <https://doi.org/10.1038/s41598-018-34651-w>.
- Decesari, S, Paglione, M, Rinaldi, M, Dall'Osto, M, Simó, R, Zanca, N, Volpi, F, Facchini, MC, Hoffmann, T, Götz, S, Kampf, CJ, O'Dowd, C, Ceburnis, D, Ovadnevaite, J, Tagliavini, E.** 2020. Shipborne measurements of Antarctic submicron organic aerosols: An NMR perspective linking multiple sources and bioregions. *Atmospheric Chemistry and Physics* **20**: 4193–4207. DOI: <https://doi.org/10.5194/acp-20-4193-2020>.
- DeMott, PJ, Hill, TCJ, McCluskey, CS, Prather, KA, Collins, DB, Sullivan, RC, Ruppel, MJ, Mason, RH, Irish, VE, Lee, T, Hwang, CY, Rhee, TS, Snider, JR, McMeeking, GR, Dhaniyala, S, Lewis, ER, Wentzell, JJB, Abbatt, J, Lee, C, Sultana, CM, Ault, AP, Axson, JL, Diaz Martinez, M, Venero, I, Santos-Figueroa, G, Stokes, MD, Deane, GB, Mayol-Bracero, OL, Grassian, VH, Bertram, TH, Bertram, AK, Moffett, BF, Franc, GD.** 2016. Sea spray aerosol as a unique source of ice nucleating particles. *Proceedings of the National Academy of Sciences USA* **113**: 5797–5803. DOI: <https://doi.org/10.1073/pnas.1514034112>.
- Dickson, A, Chris, S, Christian, JR.** 2007. SOP7—Determination of dissolved organic carbon and total dissolved nitrogen in sea water, in Dickson, AG, Sabine, CL, Christian, JR eds., *Guide to best practices for ocean CO₂ measurements*. PICES Special Publication 3. British Columbia, Canada: North Pacific Marine Science Organization: 1–5.
- Durand, MD, Olson, RJ.** 1996. Contributions of phytoplankton light scattering and cell concentration changes to diel variations in beam attenuation in the equatorial Pacific from flow cytometric measurements of pico-, ultra- and nanoplankton. *Deep Sea Research Part II: Topical Studies in Oceanography* **43**: 891–906. DOI: [https://doi.org/10.1016/0967-0645\(96\)00020-3](https://doi.org/10.1016/0967-0645(96)00020-3).
- Eicken, H, Reimnitz, E, Alexandrov, V, Martin, T, Kassens, H, Viehoff, T.** 1997. Sea-ice processes in the Laptev Sea and their importance for sediment export. *Continental Shelf Research* **17**: 205–233. DOI: [https://doi.org/10.1016/S0278-4343\(96\)00024-6](https://doi.org/10.1016/S0278-4343(96)00024-6).
- Eom, H-J, Gupta, D, Cho, H-R, Hwang, HJ, Hur, SD, Gim, Y, Ro, C-U.** 2016. Single-particle investigation of summertime and wintertime Antarctic sea spray aerosols using low-Z particle EPMA, Raman microspectrometry, and ATR-FTIR imaging techniques. *Atmospheric Chemistry and Physics* **16**: 13823–13836. DOI: <https://doi.org/10.5194/acp-16-13823-2016>.
- Facchini, MC, Rinaldi, M, Decesari, S, Carbone, C, Finessi, E, Mircea, M, Fuzzi, S, Ceburnis, D, Flanagan, R, Nilsson, ED, de Leeuw, G, Martino, M, Woeltjen, J, O'Dowd, CD.** 2008. Primary submicron marine aerosol dominated by insoluble organic colloids and aggregates. *Geophysical Research Letters* **35**: 1–5. DOI: <https://doi.org/10.1029/2008gl034210>.
- Falk-Petersen, S, Sargent, JR, Henderson, J, Hegseth, EN, Hop, H, Okolodkov, YB.** 1998. Lipids and fatty acids in ice algae and phytoplankton from the Marginal Ice Zone in the Barents Sea. *Polar Biology* **20**: 41–47. DOI: <https://doi.org/10.1007/s003000050274>.
- Forestieri, SD, Moore, KA, Martinez Borrero, R, Wang, A, Stokes, MD, Cappa, CD.** 2018. Temperature and composition dependence of sea spray aerosol production. *Geophysical Research Letters* **45**: 7218–7225. DOI: <https://doi.org/10.1029/2018GL078193>.
- Fraund, M, Pham, DQ, Bonanno, D, Harder, TH, Wang, B, Brito, J, de Sá, SS, Carbone, S, China, S, Artaxo, P, Martin, ST, Pöhlker, C, Andreae, MO, Laskin, A, Gilles, MK, Moffet, RC.** 2017. Elemental mixing state of aerosol particles collected in Central Amazonia during GoAmazon2014/15. *Atmosphere* **8**: 173.
- Frossard, AA, Russell, LM, Burrows, SM, Elliott, SM, Bates, TS, Quinn, PK.** 2014. Sources and composition of submicron organic mass in marine aerosol particles. *Journal of Geophysical Research:*

- Atmospheres* **119**: 12977–13003. DOI: <https://doi.org/10.1002/2014JD021913>.
- Fu, P, Kawamura, K, Chen, J, Qin, M, Ren, L, Sun, Y, Wang, Z, Barrie, LA, Tachibana, E, Ding, A, Yamashita, Y.** 2015. Fluorescent water-soluble organic aerosols in the High Arctic atmosphere. *Scientific Reports* **5**: 9845. DOI: <https://doi.org/10.1038/srep09845>.
- Fu, PQ, Kawamura, K, Chen, J, Charrière, B, Sempéré, R.** 2013. Organic molecular composition of marine aerosols over the Arctic Ocean in summer: Contributions of primary emission and secondary aerosol formation. *Biogeosciences* **10**: 653–667. DOI: <https://doi.org/10.5194/bg-10-653-2013>.
- Fuentes, E, Coe, H, Green, D, de Leeuw, G, McFiggans, G.** 2010. Laboratory-generated primary marine aerosol via bubble-bursting and atomization. *Atmospheric Measurement Techniques* **3**: 141–162. DOI: <https://doi.org/10.5194/amt-3-141-2010>.
- Galgani, L, Piontek, J, Engel, A.** 2016. Biopolymers form a gelatinous microlayer at the air-sea interface when Arctic sea ice melts. *Scientific Reports* **6**: 29465. DOI: <https://doi.org/10.1038/srep29465>.
- Gantt, B, Meskhidze, N, Facchini, MC, Rinaldi, M, Ceburnis, D, O'Dowd, CD.** 2011. Wind speed dependent size-resolved parameterization for the organic mass fraction of sea spray aerosol. *Atmospheric Chemistry and Physics* **11**: 8777–8790. DOI: <https://doi.org/10.5194/acp-11-8777-2011>.
- Gao, Q, Leck, C, Rauschenberg, C, Matrai, PA.** 2012. On the chemical dynamics of extracellular polysaccharides in the high Arctic surface microlayer. *Ocean Science* **8**: 401–418. DOI: <https://doi.org/10.5194/os-8-401-2012>.
- Hansell, DA.** 2005. Dissolved organic carbon reference material program. *Eos, Transactions American Geophysical Union* **86**: 318–318. DOI: <https://doi.org/10.1029/2005EO350003>.
- Hansell, DA.** 2013. Recalcitrant dissolved organic carbon fractions. *Annual Review of Marine Science* **5**: 421–445. DOI: <https://doi.org/10.1146/annurev-marine-120710-100757>.
- Hara, K, Osada, K, Nishita, C, Yamagata, S, Yamano-cuhi, T, Herber, A, Matsunaga, K, Iwasaka, Y, Nagatani, M, Nakata, H.** 2002. Vertical variations of sea-salt modification in the boundary layer of spring Arctic during the ASTAR 2000 campaign. *Tellus B: Chemical and Physical Meteorology* **54**: 361–376. DOI: <https://doi.org/10.1034/j.1600-0889.2002.201253.x>.
- Hartmann, M, Adachi, K, Eppers, O, Haas, C, Herber, A, Holzinger, R, Hünnerbein, A, Jäkel, E, Jentsch, C, van Pinxteren, M, Wex, H, Willmes, S, Stratmann, F.** 2020. Wintertime airborne measurements of ice nucleating particles in the High Arctic: A hint to a marine, biogenic source for ice nucleating particles. *Geophysical Research Letters* **47**: e2020GL087770. DOI: <https://doi.org/10.1029/2020GL087770>.
- Hasenecz, ES, Jayarathne, T, Pendergraft, MA, Santander, MV, Mayer, KJ, Sauer, J, Lee, C, Gibson, WS, Kruse, SM, Malfatti, F, Prather, KA, Stone, EA.** 2020. Marine bacteria affect saccharide enrichment in sea spray aerosol during a phytoplankton bloom. *ACS Earth and Space Chemistry* **4**: 1638–1649. DOI: <https://doi.org/10.1021/acsearthspacechem.0c00167>.
- Hawkins, LN, Russell, LM.** 2010. Polysaccharides, proteins, and phytoplankton fragments: Four chemically distinct types of marine primary organic aerosol classified by single particle spectromicroscopy. *Advances in Meteorology* **2010**: 612132. DOI: <https://doi.org/10.1155/2010/612132>.
- Henderson, R, Hegseth, E, Park, M.** 1998. Seasonal variation in lipid and fatty acid composition of ice algae from the Barents Sea. *Polar Biology* **20**: 48–55. DOI: <https://doi.org/10.1007/s003000050275>.
- Hertkorn, N, Benner, R, Frommberger, M, Schmitt-Kopplin, P, Witt, M, Kaiser, K, Kettrup, A, Hedges, JI.** 2006. Characterization of a major refractory component of marine dissolved organic matter. *Geochimica et Cosmochimica Acta* **70**: 2990–3010. DOI: <https://doi.org/10.1016/j.gca.2006.03.021>.
- Hoffman, EJ, Duce, RA.** 1976. Factors influencing the organic carbon content of marine aerosols: A laboratory study. *Journal of Geophysical Research* **81**: 3667–3670. DOI: <https://doi.org/10.1029/JC081i021p03667>.
- Holm-Hansen, O, Lorenzen, CJ, Holmes, RW, Strickland, JDH.** 1965. Fluorometric determination of chlorophyll. *ICES Journal of Marine Science* **30**: 3–15. DOI: <https://doi.org/10.1093/icesjms/30.1.3>.
- Huang, C, Jiang, Q, Yao, L, Yang, H, Lin, C, Huang, T, Zhu, AX, Zhang, Y.** 2018. Variation pattern of particulate organic carbon and nitrogen in oceans and inland waters. *Biogeosciences* **15**: 1827–1841. DOI: <https://doi.org/10.5194/bg-15-1827-2018>.
- Hultin, KAH, Nilsson, ED, Krejci, R, Mårtensson, EM, Ehn, M, Hagström, Å, de Leeuw, G.** 2010. In situ laboratory sea spray production during the Marine Aerosol Production 2006 cruise on the northeastern Atlantic Ocean. *Journal of Geophysical Research: Atmospheres* **115**: D06201. DOI: <https://doi.org/10.1029/2009JD012522>.
- Ickes, L, Porter, GCE, Wagner, R, Adams, MP, Bierbauer, S, Bertram, AK, Bilde, M, Christiansen, S, Ekman, AML, Gorokhova, E, Höhler, K, Kiselev, AA, Leck, C, Möhler, O, Murray, BJ, Schiebel, T, Ullrich, R, Salter, ME.** 2020. The ice-nucleating activity of Arctic sea surface microlayer samples and marine algal cultures. *Atmospheric Chemistry and Physics* **20**: 11089–11117. DOI: <https://doi.org/10.5194/acp-20-11089-2020>.
- Irish, VE, Elizondo, P, Chen, J, Chou, C, Charette, J, Lizotte, M, Ladino, LA, Wilson, TW, Gosselin, M, Murray, BJ, Polishchuk, E, Abbatt, JPD, Miller, LA, Bertram, AK.** 2017. Ice-nucleating particles in Canadian Arctic sea-surface microlayer and bulk seawater. *Atmospheric Chemistry and Physics* **17**:

- 10583–10595. DOI: <https://doi.org/10.5194/acp-17-10583-2017>.
- Jayarathne, T, Sultana, CM, Lee, C, Malfatti, F, Cox, JL, Pendergraft, MA, Moore, KA, Azam, F, Tivanski, AV, Cappa, CD, Bertram, TH, Grassian, VH, Prather, KA, Stone, EA. 2016. Enrichment of saccharides and divalent cations in sea spray aerosol during two phytoplankton blooms. *Environmental Science & Technology* **50**: 11511–11520. DOI: <https://doi.org/10.1021/acs.est.6b02988>.
- Johannessen, OM, Shalina, EV, Miles, MW. 1999. Satellite evidence for an Arctic sea ice cover in transformation. *Science* **286**: 1937–1939. DOI: <https://doi.org/10.1126/science.286.5446.1937>.
- Johnson, BD, Wangersky, PJ. 1987. Microbubbles: Stabilization by monolayers of adsorbed particles. *Journal of Geophysical Research: Oceans* **92**: 14641–14647. DOI: <https://doi.org/10.1029/JC092iC13p14641>.
- Kammer, M, Hedrich, R, Ehrlich, H, Popp, J, Brunner, E, Krafft, C. 2010. Spatially resolved determination of the structure and composition of diatom cell walls by Raman and FTIR imaging. *Analytical and Bioanalytical Chemistry* **398**: 509–517. DOI: <https://doi.org/10.1007/s00216-010-3924-0>.
- Karlsson, L, Zieger, P. 2020. Aerosol particle number size distribution data collected during the Arctic Ocean 2018 expedition [dataset]. Dataset Version 1. Stockholm, Sweden: Bolin Centre Database. DOI: <https://doi.org/10.17043/oden-ao-2018-aerosol-dmps-1>.
- Keene, WC, Maring, H, Maben, JR, Kieber, DJ, Pszenny, AAP, Dahl, EE, Izaguirre, MA, Davis, AJ, Long, MS, Zhou, X, Smoydzin, L, Sander, R. 2007. Chemical and physical characteristics of nascent aerosols produced by bursting bubbles at a model air-sea interface. *Journal of Geophysical Research: Atmospheres* **112**. DOI: <https://doi.org/10.1029/2007JD008464>.
- Khlystov, A, Stanier, C, Pandis, SN. 2004. An algorithm for combining electrical mobility and aerodynamic size distributions data when measuring ambient aerosol special issue of Aerosol Science and Technology on findings from the Fine Particulate Matter Supersites Program. *Aerosol Science and Technology* **38**: 229–238. DOI: <https://doi.org/10.1080/02786820390229543>.
- Kieber, DJ, Keene, WC, Frossard, AA, Long, M, Maben, JR, Russell, LM, Kinsey, JD, Tyssebotn, IMB, Quinn, PK, Bates, TS. 2016. Coupled ocean-atmosphere loss of marine refractory dissolved organic carbon. *Geophysical Research Letters* **43**: 2765–2772. DOI: <https://doi.org/10.1002/2016gl068273>.
- Kim, HS, Waqued, SC, Nodurft, DT, Devarenne, TP, Yakovlev, VV, Han, A. 2017. Raman spectroscopy compatible PDMS droplet microfluidic culture and analysis platform towards on-chip lipidomics. *Analyst* **142**: 1054–1060. DOI: <https://doi.org/10.1039/C6AN02221A>.
- Kim, J-H, Moon, W, Wells, AJ, Wilkinson, JP, Langton, T, Hwang, B, Granskog, MA, Rees Jones, DW. 2018. Salinity control of thermal evolution of late summer melt ponds on Arctic sea ice. *Geophysical Research Letters* **45**: 8304–8313. DOI: <https://doi.org/10.1029/2018GL078077>.
- Kirpes, RM, Bonanno, D, May, NW, Fraund, M, Barget, AJ, Moffet, RC, Ault, AP, Pratt, KA. 2019. Winter-time Arctic sea spray aerosol composition controlled by sea ice lead microbiology. *ACS Central Science* **5**: 1760–1767. DOI: <https://doi.org/10.1021/acscentsci.9b00541>.
- Kirpes, RM, Bondy, AL, Bonanno, D, Moffet, RC, Wang, B, Laskin, A, Ault, AP, Pratt, KA. 2018. Secondary sulfate is internally mixed with sea spray aerosol and organic aerosol in the winter Arctic. *Atmospheric Chemistry and Physics* **18**: 3937–3949. DOI: <https://doi.org/10.5194/acp-18-3937-2018>.
- Kirpes, RM, Rodriguez, B, Kim, S, China, S, Laskin, A, Park, K, Jung, J, Ault, AP, Pratt, KA. 2020. Emerging investigator series: Influence of marine emissions and atmospheric processing on individual particle composition of summertime Arctic aerosol over the Bering Strait and Chukchi Sea. *Environmental Science: Processes & Impacts* **22**: 1201–1213. DOI: <https://doi.org/10.1039/C9EM00495E>.
- Klunder, MB, Bauch, D, Laan, P, de Baar, HJW, van Heuven, S, Ober, S. 2012. Dissolved iron in the Arctic shelf seas and surface waters of the central Arctic Ocean: Impact of Arctic river water and ice-melt. *Journal of Geophysical Research: Oceans* **117**. DOI: <https://doi.org/10.1029/2011JC007133>.
- Kohlbach, D, Duerksen, SW, Lange, BA, Charette, J, Reppchen, A, Tremblay, P, Campbell, KL, Ferguson, SH, Michel, C. 2020. Fatty acids and stable isotope signatures of first-year and multiyear sea ice in the Canadian High Arctic. *Elementa: Science of the Anthropocene* **8**. DOI: <https://doi.org/10.1525/elementa.2020.054>.
- Kohlbach, D, Graeve, M, Lange, BA, David, C, Peeken, I, Flores, H. 2016. The importance of ice algae-produced carbon in the central Arctic Ocean ecosystem: Food web relationships revealed by lipid and stable isotope analyses. *Limnology and Oceanography* **61**: 2027–2044. DOI: <https://doi.org/10.1002/lno.10351>.
- Kuznetsova, M, Lee, C, Aller, J. 2005. Characterization of the proteinaceous matter in marine aerosols. *Marine Chemistry* **96**: 359–377. DOI: <https://doi.org/10.1016/j.marchem.2005.03.007>.
- Lannuzel, D, Tedesco, L, van Leeuwe, M, Campbell, K, Flores, H, Delille, B, Miller, L, Stefels, J, Assmy, P, Bowman, J, Brown, K, Castellani, G, Chierici, M, Crabeck, O, Damm, E, Else, B, Fransson, A, Fripiat, F, Geilfus, N-X, Jacques, C, Jones, E, Kaartokallio, H, Kotovitch, M, Meiners, K, Moreau, S, Nomura, D, Peeken, I, Rintala, J-M, Steiner, N, Tison, J-L, Vancoppenolle, M, Van der Linden, F, Vichi, M, Wongpan, P. 2020. The future of Arctic sea-ice biogeochemistry and ice-associated ecosystems. *Nature Climate Change* **10**: 983–992. DOI: <https://doi.org/10.1038/s41558-020-00940-4>.
- Laskin, A, Iedema, MJ, Cowin, JP. 2002. Quantitative time-resolved monitoring of nitrate formation in

- sea salt particles using a CCSEM/EDX single particle analysis. *Environmental Science & Technology* **36**: 4948–4955. DOI: <https://doi.org/10.1021/es020551k>.
- Laskina, O, Morris, HS, Grandquist, JR, Estillore, AD, Stone, EA, Grassian, VH, Tivanski, AV.** 2015. Substrate-deposited sea spray aerosol particles: Influence of analytical method, substrate, and storage conditions on particle size, phase, and morphology. *Environmental Science & Technology* **49**: 13447–13453. DOI: <https://doi.org/10.1021/acs.est.5b02732>.
- Lawler, MJ, Lewis, SL, Russell, LM, Quinn, PK, Bates, TS, Coffman, DJ, Upchurch, LM, Saltzman, ES.** 2020. North Atlantic marine organic aerosol characterized by novel offline thermal desorption mass spectrometry: Polysaccharides, recalcitrant material, and secondary organics. *Atmospheric Chemistry and Physics* **20**: 16007–16022. DOI: <https://doi.org/10.5194/acp-20-16007-2020>.
- Leck, C, Gao, Q, Mashayekhy Rad, F, Nilsson, U.** 2013. Size-resolved atmospheric particulate polysaccharides in the high summer Arctic. *Atmospheric Chemistry and Physics* **13**: 12573–12588. DOI: <https://doi.org/10.5194/acp-13-12573-2013>.
- Leck, C, Norman, M, Bigg, EK, Hillamo, R.** 2002. Chemical composition and sources of the high Arctic aerosol relevant for cloud formation. *Journal of Geophysical Research: Atmospheres* **107**: AAC 1-1–AAC 1-17. DOI: <https://doi.org/10.1029/2001JD001463>.
- Letscher, RT, Hansell, DA, Kadko, D, Bates, NR.** 2013. Dissolved organic nitrogen dynamics in the Arctic Ocean. *Marine Chemistry* **148**: 1–9. DOI: <https://doi.org/10.1016/j.marchem.2012.10.002>.
- Lin, S.** 2011. Genomic understanding of dinoflagellates. *Research in Microbiology* **162**: 551–569. DOI: <https://doi.org/10.1016/j.resmic.2011.04.006>.
- Liu, S, Liu, C-C, Froyd, KD, Schill, GP, Murphy, DM, Bui, TP, Dean-Day, JM, Weinzierl, B, Dollner, M, Diskin, GS, Chen, G, Gao, R-S.** 2021. Sea spray aerosol concentration modulated by sea surface temperature. *Proceedings of the National Academy of Sciences* **118**: e2020583118. DOI: <https://doi.org/10.1073/pnas.2020583118>.
- Logvinova, CL, Frey, KE, Cooper, LW.** 2016. The potential role of sea ice melt in the distribution of chromophoric dissolved organic matter in the Chukchi and Beaufort Seas. *Deep Sea Research Part II: Topical Studies in Oceanography* **130**: 28–42. DOI: <https://doi.org/10.1016/j.dsr2.2016.04.017>.
- Lomas, MW, Steinberg, DK, Dickey, T, Carlson, CA, Nelson, NB, Condon, RH, Bates, NR.** 2010. Increased ocean carbon export in the Sargasso Sea linked to climate variability is countered by its enhanced mesopelagic attenuation. *Biogeosciences* **7**: 57–70. DOI: <https://doi.org/10.5194/bg-7-57-2010>.
- Lv, C, Tsona, NT, Du, L.** 2020. Sea spray aerosol formation: Results on the role of different parameters and organic concentrations from bubble bursting experiments. *Chemosphere* **252**: 126456. DOI: <https://doi.org/10.1016/j.chemosphere.2020.126456>.
- Marie, D, Simon, N, Vulot, D.** 2005. Phytoplankton cell counting by flow cytometry, in Andersen, RA ed., *Algal culturing techniques*. New York, NY: Elsevier Academic Press: 253–267.
- Mårtensson, EM, Nilsson, ED, de Leeuw, G, Cohen, LH, Hansson, HC.** 2003. Laboratory simulations and parameterization of the primary marine aerosol production. *Journal of Geophysical Research: Atmospheres* **108**. DOI: <https://doi.org/10.1029/2002JD002263>.
- May, NW, Axson, JL, Watson, A, Pratt, KA, Ault, AP.** 2016a. Lake spray aerosol generation: A method for producing representative particles from freshwater wave breaking. *Atmospheric Measurement Techniques* **9**: 4311–4325. DOI: <https://doi.org/10.5194/amt-9-4311-2016>.
- May, NW, Quinn, PK, McNamara, SM, Pratt, KA.** 2016b. Multiyear study of the dependence of sea salt aerosol on wind speed and sea ice conditions in the coastal Arctic. *Journal of Geophysical Research: Atmospheres* **121**: 9208–9219. DOI: <https://doi.org/10.1002/2016JD025273>.
- Mayer, KJ, Sauer, JS, Dinasquet, J, Prather, KA.** 2020. CAICE studies: Insights from a decade of ocean–atmosphere experiments in the laboratory. *Accounts of Chemical Research* **53**: 2510–2520. DOI: <https://doi.org/10.1021/acs.accounts.0c00504>.
- McCluskey, CS, Hill, TCJ, Humphries, RS, Rauker, AM, Moreau, S, Stratton, PG, Chambers, SD, Williams, AG, McRobert, I, Ward, J, Keywood, MD, Harnwell, J, Ponsonby, W, Loh, ZM, Krummel, PB, Protat, A, Kreidenweis, SM, DeMott, PJ.** 2018. Observations of ice nucleating particles over Southern Ocean waters. *Geophysical Research Letters* **45**: 11989–11997. DOI: <https://doi.org/10.1029/2018GL079981>.
- Measures, CI.** 1999. The role of entrained sediments in sea ice in the distribution of aluminium and iron in the surface waters of the Arctic Ocean. *Marine Chemistry* **68**: 59–70. DOI: [https://doi.org/10.1016/S0304-4203\(99\)00065-1](https://doi.org/10.1016/S0304-4203(99)00065-1).
- Meinander, O, Dagsson-Waldhauserova, P, Amosov, P, Aseyeva, E, Atkins, C, Baklanov, A, Baldo, C, Barr, SL, Barzycka, B, Benning, LG, Cvetkovic, B, Enchilik, P, Frolov, D, Gassó, S, Kandler, K, Kasimov, N, Kavan, J, King, J, Koroleva, T, Krupskaya, V, Kullmala, M, Kusiak, M, Lappalainen, HK, Laska, M, Lasne, J, Lewandowski, M, Luks, B, McQuaid, JB, Moroni, B, Murray, B, Möhler, O, Nawrot, A, Nickovic, S, O'Neill, NT, Pejanovic, G, Popovicheva, O, Ranjbar, K, Romanias, M, Samonova, O, Sanchez-Marroquin, A, Schepanski, K, Semenkov, I, Sharapova, A, Shevnina, E, Shi, Z, Sofiev, M, Thevenet, F, Thorsteinsson, T, Timofeev, M, Umo, NS, Uppstu, A, Urupina, D, Varga, G, Werner, T, Arnalds, O, Vukovic Vimic, A.** 2022. Newly identified climatically and environmentally

- significant high-latitude dust sources. *Atmospheric Chemistry and Physics* **22**: 11889–11930. DOI: <https://doi.org/10.5194/acp-22-11889-2022>.
- Millero, FJ, Feistel, R, Wright, DG, McDougall, TJ.** 2008. The composition of Standard Seawater and the definition of the Reference-Composition Salinity Scale. *Deep Sea Research Part I: Oceanographic Research Papers* **55**: 50–72. DOI: <https://doi.org/10.1016/j.dsr.2007.10.001>.
- Mirrielees, JA, Kirpes, RM, Haas, SM, Rauschenberg, CD, Matrai, PA, Remenapp, A, Boschi, VL, Grannas, AM, Pratt, KA, Ault, AP.** 2022. Probing individual particles generated at the freshwater–seawater interface through combined Raman, photothermal infrared, and X-ray spectroscopic characterization. *ACS Measurement Science Au* **2**: 605–619. DOI: <https://doi.org/10.1021/acsmesuresciau.2c00041>.
- Mochida, M, Kitamori, Y, Kawamura, K, Nojiri, Y, Suzuki, K.** 2002. Fatty acids in the marine atmosphere: Factors governing their concentrations and evaluation of organic films on sea-salt particles. *Journal of Geophysical Research: Atmospheres* **107**: AAC 1-1–AAC 1-10. DOI: <https://doi.org/10.1029/2001JD001278>.
- Mukherjee, P, Reinfelder, JR, Gao, Y.** 2020. Enrichment of calcium in sea spray aerosol in the Arctic summer atmosphere. *Marine Chemistry* **227**: 103898. DOI: <https://doi.org/10.1016/j.marchem.2020.103898>.
- Nielsen, LS, Bilde, M.** 2020. Exploring controlling factors for sea spray aerosol production: Temperature, inorganic ions and organic surfactants. *Tellus B: Chemical and Physical Meteorology* **72**: 1–10. DOI: <https://doi.org/10.1080/16000889.2020.1801305>.
- Nilsson, ED, Rannik, Ü, Swietlicki, E, Leck, C, Aalto, PP, Zhou, J, Norman, M.** 2001. Turbulent aerosol fluxes over the Arctic Ocean: 2. Wind-driven sources from the sea. *Journal of Geophysical Research: Atmospheres* **106**: 32139–32154. DOI: <https://doi.org/10.1029/2000JD900747>.
- Norris, SJ, Brooks, IM, de Leeuw, G, Sirevaag, A, Leck, C, Brooks, BJ, Birch, CE, Tjernström, M.** 2011. Measurements of bubble size spectra within leads in the Arctic summer pack ice. *Ocean Science* **7**: 129–139. DOI: <https://doi.org/10.5194/os-7-129-2011>.
- Nürnberg, D, Wollenburg, I, Dethleff, D, Eicken, H, Kassens, H, Letzig, T, Reimnitz, E, Thiede, J.** 1994. Sediments in Arctic sea ice: Implications for entrainment, transport and release. *Marine Geology* **119**: 185–214. DOI: [https://doi.org/10.1016/0025-3227\(94\)90181-3](https://doi.org/10.1016/0025-3227(94)90181-3).
- O'Dowd, C, Ceburnis, D, Ovadnevaite, J, Bialek, J, Stengel, DB, Zacharias, M, Nitschke, U, Connan, S, Rinaldi, M, Fuzzi, S, Decesari, S, Facchini, MC, Marullo, S, Santolero, R, Dell'Anno, A, Corinaldesi, C, Tangherlini, M, Danovaro, R.** 2015. Connecting marine productivity to sea-spray via nanoscale biological processes: Phytoplankton dance or death disco? *Scientific Reports* **5**: 14883. DOI: <https://doi.org/10.1038/srep14883>.
- O'Dowd, CD, Facchini, MC, Cavalli, F, Ceburnis, D, Mircea, M, Decesari, S, Fuzzi, S, Yoon, YJ, Putaud, J-P.** 2004. Biogenically driven organic contribution to marine aerosol. *Nature* **431**: 676–680. DOI: <https://doi.org/10.1038/nature02959>.
- Orellana, MV, Hansell, DA, Matrai, PA, Leck, C.** 2021. Marine polymer-gels' relevance in the atmosphere as aerosols and CCN. *Gels* **7**: 185.
- Orellana, MV, Leck, C.** 2015. Marine microgels, in Hansell, DA, Carlson, CA eds., *Biogeochemistry of marine dissolved organic matter. 2nd ed.* London, UK: Elsevier Academic Press: 451–480. DOI: <https://doi.org/10.1016/b978-0-12-405940-5.00009-1>.
- O'Sullivan, D, Adams, MP, Tarn, MD, Harrison, AD, Vergara-Temprado, J, Porter, GC, Holden, MA, Sanchez-Marroquin, A, Carotenuto, F, Whale, TF, McQuaid, JB.** 2018. Contributions of biogenic material to the atmospheric ice-nucleating particle population in North Western Europe. *Scientific Reports* **8**: 13821. DOI: <https://doi.org/10.1038/s41598-018-31981-7>.
- Overland, J, Dunlea, E, Box, JE, Corell, R, Forsius, M, Kattsov, V, Olsen, MS, Pawlak, J, Reiersen, L-O, Wang, M.** 2019. The urgency of Arctic change. *Polar Science* **21**: 6–13. DOI: <https://doi.org/10.1016/j.polar.2018.11.008>.
- Overland, JE, Wang, M.** 2013. When will the summer Arctic be nearly sea ice free? *Geophysical Research Letters* **40**: 2097–2101. DOI: <https://doi.org/10.1002/grl.50316>.
- Pachauri, RK, Allen, MR, Barros, VR, Broome, J, Cramer, W, Christ, R, Church, JA, Clarke, L, Dahe, Q, Dasgupta, P, Dubash, NK, Edenhofer, O, Elgizouli, I, Field, CB, Forster, P, Friedlingstein, P, Fuglestvedt, J, Gomez-Echeverri, L, Hallegatte, S, Hegerl, G, Howden, M, Jiang, K, Jimenez Cisneroz, B, Kattsov, V, Lee, H, Mach, KJ, Marotzke, J, Mastrandrea, MD, Meyer, L, Minx, J, Muloggetta, Y, O'Brien, K, Oppenheimer, M, Pereira, JJ, Pichs-Madruga, R, Plattner, G-K, Pörtner, HO, Power, SB, Preston, B, Ravindranath, NH, Reisinger, A, Riahi, K, Rusticucci, M, Scholes, R, Seyboth, K, Sokona, Y, Stavins, R, Stocker, TF, Tschakert, P, van Vuuren, D, van Ypserle, J-P.** 2014. Climate Change 2014: Synthesis Report. Contribution of Working Groups I, II and III to the Fifth Assessment Report of the Intergovernmental Panel on Climate Change. Geneva, Switzerland: IPCC: 151 pp. ISBN: 978-92-9169-143-2.
- Park, J, Dall'Osto, M, Park, K, Kim, J-H, Park, J, Park, K-T, Hwang, CY, Jang, G II, Gim, Y, Kang, S, Park, S, Jin, YK, Yum, SS, Simó, R, Yoon, YJ.** 2019a. Arctic primary aerosol production strongly influenced by riverine organic matter. *Environmental Science & Technology* **53**: 8621–8630. DOI: <https://doi.org/10.1021/acs.est.9b03399>.
- Park, K, Kim, I, Choi, J-O, Lee, Y, Jung, J, Ha, S-Y, Kim, J-H, Zhang, M.** 2019b. Unexpectedly high dimethyl sulfide concentration in high-latitude Arctic sea ice melt ponds. *Environmental Science: Processes*

- & *Impacts* **21**. DOI: <https://doi.org/10.1039/C9EM00195F>.
- Pilson, MEQ.** 2013. Major constituents of seawater, in Pilson, MEQ ed., *An introduction to the chemistry of the sea. 2nd ed.* Cambridge, UK: Cambridge University Press: 66–73. DOI: <https://doi.org/10.1017/CBO9781139047203>.
- Pinzaru, SC, Müller, C, Tomšić, S, Venter, MM, Brezestean, I, Ljubimir, S, Glamuzina, B.** 2016. Live diatoms facing Ag nanoparticles: Surface enhanced Raman scattering of bulk *Cylindrotheca closterium* pennate diatoms and of the single cells. *RSC Advances* **6**: 42899–42910. DOI: <https://doi.org/10.1039/C6RA04255D>.
- Porter, GCE, Adams, MP, Brooks, IM, Ickes, L, Karlsson, L, Leck, C, Salter, ME, Schmale, J, Siegel, K, Sikora, SNF, Tarn, MD, Vüllers, J, Wernli, H, Zieger, P, Zinke, J, Murray, BJ.** 2022. Highly active ice-nucleating particles at the summer North Pole. *Journal of Geophysical Research: Atmospheres* **127**: e2021JD036059. DOI: <https://doi.org/10.1029/2021JD036059>.
- Poulin, M, Daughjerg, N, Gradinger, R, Ilyash, L, Ratkova, T, von Quillfeldt, C.** 2011. The pan-Arctic biodiversity of marine pelagic and sea-ice unicellular eukaryotes: A first-attempt assessment. *Marine Biodiversity* **41**: 13–28. DOI: <https://doi.org/10.1007/s12526-010-0058-8>.
- Poulton, N.** 2023. Sample fixation procedure for pico/nanoplankton flow cytometry. Center for Aquatic Cytometry, Bigelow Laboratory. Available at https://www.bigelow.org/services/fac/files/SOP001_PicoNano_Fixation_20230606.pdf. Accessed June 6, 2023.
- Prather, KA, Bertram, TH, Grassian, VH, Deane, GB, Stokes, MD, DeMott, PJ, Aluwihare, LI, Palenik, BP, Azam, F, Seinfeld, JH, Moffet, RC, Molina, MJ, Cappa, CD, Geiger, FM, Roberts, GC, Russell, LM, Ault, AP, Baltrusaitis, J, Collins, DB, Corrigan, CE, Cuadra-Rodriguez, LA, Ebben, CJ, Forestieri, SD, Guasco, TL, Hersey, SP, Kim, MJ, Lambert, WF, Modini, RL, Mui, W, Pedler, BE, Ruppel, MJ, Ryder, OS, Schoepp, NG, Sullivan, RC, Zhao, D.** 2013. Bringing the ocean into the laboratory to probe the chemical complexity of sea spray aerosol. *Proceedings of the National Academy of Sciences USA* **110**: 7550–7555. DOI: <https://doi.org/10.1073/pnas.1300262110>.
- Prytherch, J, Tjernström, M.** 2019. Navigation, meteorological and surface seawater data from the Arctic Ocean 2018 expedition [dataset]. Dataset Version 1. DOI: <https://doi.org/10.17043/oden-ao-2018-navigation-1>.
- Qu, M, Pang, X, Zhao, X, Lei, R, Ji, Q, Liu, Y, Chen, Y.** 2021. Spring leads in the Beaufort Sea and its inter-annual trend using Terra/MODIS thermal imagery. *Remote Sensing of Environment* **256**: 112342. DOI: <https://doi.org/10.1016/j.rse.2021.112342>.
- Quinn, PK, Bates, TS, Schulz, KS, Coffman, DJ, Frossard, AA, Russell, LM, Keene, WC, Kieber, DJ.** 2014. Contribution of sea surface carbon pool to organic matter enrichment in sea spray aerosol. *Nature Geosciences* **7**: 228–232. DOI: <https://doi.org/10.1038/ngeo2092>.
- Quinn, PK, Collins, DB, Grassian, VH, Prather, KA, Bates, TS.** 2015. Chemistry and related properties of freshly emitted sea spray aerosol. *Chemical Reviews* **115**: 4383–4399. DOI: <https://doi.org/10.1021/cr500713g>.
- Radke, LF, Hobbs, PV, Pinnons, JE.** 1976. Observations of cloud condensation nuclei, sodium-containing particles, ice nuclei and the light-scattering coefficient near Barrow, Alaska. *Journal of Applied Meteorology and Climatology* **15**: 982–995. DOI: [https://doi.org/10.1175/1520-0450\(1976\)015<0982:OCCNS>2.0.CO;2](https://doi.org/10.1175/1520-0450(1976)015<0982:OCCNS>2.0.CO;2).
- Rantanen, M, Karpechko, AY, Lipponen, A, Nordling, K, Hyvärinen, O, Ruosteenoja, K, Vihma, T, Laaksonen, A.** 2022. The Arctic has warmed nearly four times faster than the globe since 1979. *Communications Earth & Environment* **3**: 168. DOI: <https://doi.org/10.1038/s43247-022-00498-3>.
- Reimnitz, E, Barnes, PW, Weber, WS.** 1993. Particulate matter in pack ice of the Beaufort Gyre. *Journal of Glaciology* **39**: 186–198. DOI: <https://doi.org/10.3189/S0022143000015823>.
- Ribeiro, J, Lima, RA.** 2022. Applications of polydimethylsiloxane (PDMS) in engineering. *Journal of Functional Biomaterials* **13**: 2.
- Richter-Menge, JA, Farrell, SL.** 2013. Arctic sea ice conditions in spring 2009–2013 prior to melt. *Geophysical Research Letters* **40**: 5888–5893. DOI: <https://doi.org/10.1002/2013GL058011>.
- Rocchi, A, von Jackowski, A, Welti, A, Li, G, Kanji, ZA, Povazhnyy, V, Engel, A, Schmale, J, Nenes, A, Berdalet, E, Simó, R, Dall'Osto, M.** 2024. Glucose enhances salinity-driven sea spray aerosol production in eastern Arctic waters. *Environmental Science & Technology* **58**: 8748–8759. DOI: <https://doi.org/10.1021/acs.est.4c02826>.
- Rüger, J, Unger, N, Schie, IW, Brunner, E, Popp, J, Krafft, C.** 2016. Assessment of growth phases of the diatom *Ditylum brightwellii* by FT-IR and Raman spectroscopy. *Algal Research* **19**: 246–252. DOI: <https://doi.org/10.1016/j.algal.2016.09.007>.
- Russell, LM, Moore, RH, Burrows, SM, Quinn, PK.** 2023. Ocean flux of salt, sulfate, and organic components to atmospheric aerosol. *Earth-Science Reviews* **239**: 104364. DOI: <https://doi.org/10.1016/j.earscirev.2023.104364>.
- Salter, ME, Hamacher-Barth, E, Leck, C, Werner, J, Johnson, CM, Riipinen, I, Nilsson, ED, Zieger, P.** 2016. Calcium enrichment in sea spray aerosol particles. *Geophysical Research Letters* **43**: 8277–8285. DOI: <https://doi.org/10.1002/2016GL070275>.
- Salter, ME, Nilsson, ED, Butcher, A, Bilde, M.** 2014. On the seawater temperature dependence of the sea spray aerosol generated by a continuous plunging jet. *Journal of Geophysical Research: Atmospheres*

- 119: 9052–9072. DOI: <https://doi.org/10.1002/2013JD021376>.
- Salter, ME, Zieger, P, Acosta Navarro, JC, Grythe, H, Kirkevåg, A, Rosati, B, Riipinen, I, Nilsson, ED.** 2015. An empirically derived inorganic sea spray source function incorporating sea surface temperature. *Atmospheric Chemistry and Physics* **15**: 11047–11066. DOI: <https://doi.org/10.5194/acp-15-11047-2015>.
- Sanchez-Marroquin, A, Arnalds, O, Baustian-Dorsi, KJ, Browse, J, Dagsson-Waldhauserova, P, Harrison, AD, Maters, EC, Pringle, KJ, Vergara-Temprado, J, Burke, IT, McQuaid, JB, Carslaw, KS, Murray, BJ.** 2020. Iceland is an episodic source of atmospheric ice-nucleating particles relevant for mixed-phase clouds. *Science Advances* **6**: eaba8137. DOI: <https://doi.org/10.1126/sciadv.aba8137>.
- Santander, MV, Mitts, BA, Pendergraft, MA, Dinasquet, J, Lee, C, Moore, AN, Cancelada, LB, Kimble, KLA, Malfatti, F, Prather, KA.** 2021. Tandem fluorescence measurements of organic matter and bacteria released in sea spray aerosols. *Environmental Science & Technology* **55**: 5171–5179. DOI: <https://doi.org/10.1021/acs.est.0c05493>.
- Santander, MV, Schiffer, JM, Lee, C, Axson, JL, Tauber, MJ, Prather, KA.** 2022. Factors controlling the transfer of biogenic organic species from seawater to sea spray aerosol. *Scientific Reports* **12**: 3580. DOI: <https://doi.org/10.1038/s41598-022-07335-9>.
- Sauer, JS, Mayer, KJ, Lee, C, Alves, MR, Amiri, S, Bahaveolos, CJ, Franklin, EB, Crocker, DR, Dang, D, Dinasquet, J, Garofalo, LA, Kaluarachchi, CP, Kilgour, DB, Mael, LE, Mitts, BA, Moon, DR, Moore, AN, Morris, CK, Mullenmeister, CA, Ni, C-M, Pendergraft, MA, Petras, D, Simpson, RMC, Smith, S, Tumminello, PR, Walker, JL, DeMott, PJ, Farmer, DK, Goldstein, AH, Grassian, VH, Jaffe, JS, Malfatti, F, Martz, TR, Slade, JH, Tivanski, AV, Bertram, TH, Cappa, CD, Prather, KA.** 2022. The Sea Spray Chemistry and Particle Evolution study (SeaSCAPE): Overview and experimental methods. *Environmental Science: Processes & Impacts* **24**: 290–315. DOI: <https://doi.org/10.1039/D1EM00260K>.
- Scalabrin, E, Zangrando, R, Barbaro, E, Kehrwald, NM, Gabrieli, J, Barbante, C, Gambaro, A.** 2012. Amino acids in Arctic aerosols. *Atmospheric Chemistry and Physics* **12**: 10453–10463. DOI: <https://doi.org/10.5194/acp-12-10453-2012>.
- Schanke, NL, Bolinesi, F, Mangoni, O, Katlein, C, Anhaus, P, Hoppmann, M, Lee, PA, DiTullio, GR.** 2020. Biogeochemical and ecological variability during the late summer–early autumn transition at an ice-floe drift station in the central Arctic Ocean. *Limnology and Oceanography* **66**: S363–S382. DOI: <https://doi.org/10.1002/lno.11676>.
- Schwier, AN, Sellegri, K, Mas, S, Charriere, B, Pey, J, Rose, C, Temime-Roussel, B, Jaffrezo, J-L, Parin, D, Picard, D, Ribeiro, M, Roberts, G, Sempere, R, Marchand, N, D'Anna, B.** 2017. Primary marine aerosol physical flux and chemical composition during a nutrient enrichment experiment in mesocosms in the Mediterranean Sea. *Atmospheric Chemistry and Physics* **17**: 14645–14660. DOI: <https://doi.org/10.5194/acp-17-14645-2017>.
- Scott, WD, Levin, Z.** 1972. Open channels in sea ice (leads) as ion sources. *Science* **177**: 425–426.
- Serreze, MC, Stroeve, J.** 2015. Arctic sea ice trends, variability and implications for seasonal ice forecasting. *Philosophical Transactions of the Royal Society A: Mathematical, Physical and Engineering Sciences* **373**: 20140159. DOI: <https://doi.org/10.1098/rsta.2014.0159>.
- Siegel, K, Karlsson, L, Zieger, P, Baccarini, A, Schmale, J, Lawler, M, Salter, M, Leck, C, Ekman, AML, Riipinen, I, Mohr, C.** 2021. Insights into the molecular composition of semi-volatile aerosols in the summertime central Arctic Ocean using FIGAERO-CIMS. *Environmental Science: Atmospheres* **1**: 161–175. DOI: <https://doi.org/10.1039/D0EA00023J>.
- Sørensen, HL, Thamdrup, B, Jeppesen, E, Rysgaard, S, Glud, RN.** 2017. Nutrient availability limits biological production in Arctic sea ice melt ponds. *Polar Biology* **40**: 1593–1606. DOI: <https://doi.org/10.1007/s00300-017-2082-7>.
- Steinberg, DK, Carlson, C, Bates, NR, Johnson, RJ, Michaels, A, Knapp, AH.** 2001. Overview of the US JGOFS Bermuda Atlantic Time-series Study (BATS): A decade-scale look at ocean biology and biogeochemistry. *Deep Sea Research Part II: Topical Studies in Oceanography* **48**: 1405–1447. DOI: [https://doi.org/10.1016/S0967-0645\(00\)00148-X](https://doi.org/10.1016/S0967-0645(00)00148-X).
- Stokes, MD, Deane, GB, Prather, K, Bertram, TH, Ruppel, MJ, Ryder, OS, Brady, JM, Zhao, D.** 2013. A Marine Aerosol Reference Tank system as a breaking wave analogue for the production of foam and sea-spray aerosols. *Atmospheric Measurement Techniques* **6**: 1085–1094. DOI: <https://doi.org/10.5194/amt-6-1085-2013>.
- Stroeve, JC, Markus, T, Boisvert, L, Miller, J, Barrett, A.** 2014. Changes in Arctic melt season and implications for sea ice loss. *Geophysical Research Letters* **41**: 1216–1225. DOI: <https://doi.org/10.1002/2013GL058951>.
- Stroeve, JC, Serreze, MC, Holland, MM, Kay, JE, Malanik, J, Barrett, AP.** 2012. The Arctic's rapidly shrinking sea ice cover: A research synthesis. *Climatic Change* **110**: 1005–1027. DOI: <https://doi.org/10.1007/s10584-011-0101-1>.
- Struthers, H, Ekman, AML, Glantz, P, Iversen, T, Kirkevåg, A, Mårtensson, EM, Seland, Ø, Nilsson, ED.** 2011. The effect of sea ice loss on sea salt aerosol concentrations and the radiative balance in the Arctic. *Atmospheric Chemistry and Physics* **11**: 3459–3477. DOI: <https://doi.org/10.5194/acp-11-3459-2011>.
- Sumata, H, de Steur, L, Divine, DV, Granskog, MA, Gerland, S.** 2023. Regime shift in Arctic Ocean sea ice thickness. *Nature* **615**: 443–449. DOI: <https://doi.org/10.1038/s41586-022-05686-x>.

- Szymanski, A, Gradinger, R.** 2016. The diversity, abundance and fate of ice algae and phytoplankton in the Bering Sea. *Polar Biology* **39**: 309–325. DOI: <https://doi.org/10.1007/s00300-015-1783-z>.
- Tedesco, L, Vichi, M, Scocimarro, E.** 2019. Sea-ice algal phenology in a warmer Arctic. *Science Advances* **5**: eaav4830. DOI: <https://doi.org/10.1126/sciadv.aav4830>.
- Triesch, N, van Pinxteren, M, Salter, M, Stolle, C, Pereira, R, Zieger, P, Herrmann, H.** 2021. Sea spray aerosol chamber study on selective transfer and enrichment of free and combined amino acids. *ACS Earth Space Chemistry* **5**: 1564–1574. DOI: <https://doi.org/10.1021/acsearthspacechem.1c00080>.
- Tyree, CA, Hellion, VM, Alexandrova, OA, Allen, JO.** 2007. Foam droplets generated from natural and artificial seawaters. *Journal of Geophysical Research: Atmospheres* **112**. DOI: <https://doi.org/10.1029/2006JD007729>.
- van Pinxteren, M, Zeppenfeld, S, Fomba, KW, Triesch, N, Frka, S, Herrmann, H.** 2023. Amino acids, carbohydrates, and lipids in the tropical oligotrophic Atlantic Ocean: Sea-to-air transfer and atmospheric in situ formation. *Atmospheric Chemistry and Physics* **23**: 6571–6590. DOI: <https://doi.org/10.5194/acp-23-6571-2023>.
- Vaulot, D, Courties, C, Partensky, F.** 1989. A simple method to preserve oceanic phytoplankton for flow cytometric analyses. *Cytometry* **10**: 629–635. DOI: <https://doi.org/10.1002/cyto.990100519>.
- Verdugo, P.** 2012. Marine microgels. *Annual Review of Marine Science* **4**: 375–400. DOI: <https://doi.org/10.1146/annurev-marine-120709-142759>.
- Vergara-Temprado, J, Murray, BJ, Wilson, TW, O'Sullivan, D, Browse, J, Pringle, KJ, Ardon-Dryer, K, Bertram, AK, Burrows, SM, Ceburnis, D, DeMott, PJ, Mason, RH, O'Dowd, CD, Rinaldi, M, Carslaw, KS.** 2017. Contribution of feldspar and marine organic aerosols to global ice nucleating particle concentrations. *Atmospheric Chemistry and Physics* **17**: 3637–3658. DOI: <https://doi.org/10.5194/acp-17-3637-2017>.
- Vernet, M, Ellingsen, I, Marchese, C, Bélanger, S, Cape, M, Slagstad, D, Matrai, PA.** 2021. Spatial variability in rates of net primary production (NPP) and onset of the spring bloom in Greenland shelf waters. *Progress in Oceanography* **198**: 102655. DOI: <https://doi.org/10.1016/j.pocean.2021.102655>.
- Vüllers, J, Achtert, P, Brooks, IM, Tjernström, M, Prytherch, J, Burzik, A, Neely, R III.** 2021. Meteorological and cloud conditions during the Arctic Ocean 2018 expedition. *Atmospheric Chemistry and Physics* **21**: 289–314. DOI: <https://doi.org/10.5194/acp-21-289-2021>.
- Wagner, R, Ickes, L, Bertram, AK, Els, N, Gorokhova, E, Möhler, O, Murray, BJ, Umo, NS, Salter, ME.** 2021. Heterogeneous ice nucleation ability of aerosol particles generated from Arctic sea surface microlayer and surface seawater samples at cirrus temperatures. *Atmospheric Chemistry and Physics* **21**: 13903–13930. DOI: <https://doi.org/10.5194/acp-21-13903-2021>.
- Wang, XF, Sultana, CM, Trueblood, J, Hill, TCJ, Malfatti, F, Lee, C, Laskina, O, Moore, KA, Beall, CM, McCluskey, CS, Cornwell, GC, Zhou, Y, Cox, JL, Pendergraft, MA, Santander, MV, Bertram, TH, Cappa, CD, Azam, F, DeMott, PJ, Grassian, VH, Prather, KA.** 2015. Microbial control of sea spray aerosol composition: A tale of two blooms. *ACS Central Science* **1**: 124–131. DOI: <https://doi.org/10.1021/acscentsci.5b00148>.
- Weeks, W.** 2010. *On sea ice*. Fairbanks, AK: University of Alaska Press.
- Welschmeyer, NA.** 1994. Fluorometric analysis of chlorophyll *a* in the presence of chlorophyll *b* and pheopigments. *Limnology and Oceanography* **39**: 1985–1992. DOI: <https://doi.org/10.4319/lo.1994.39.8.1985>.
- Wex, H, Huang, L, Zhang, W, Hung, H, Traversi, R, Becagli, S, Sheesley, RJ, Moffett, CE, Barrett, TE, Bossi, R, Skov, H, Hünerbein, A, Lubitz, J, Löffler, M, Linke, O, Hartmann, M, Herenz, P, Stratmann, F.** 2019. Annual variability of ice-nucleating particle concentrations at different Arctic locations. *Atmospheric Chemistry and Physics* **19**: 5293–5311. DOI: <https://doi.org/10.5194/acp-19-5293-2019>.
- Whale, TF, Murray, BJ, O'Sullivan, D, Wilson, TW, Umo, NS, Baustian, KJ, Atkinson, JD, Workneh, DA, Morris, GJ.** 2015. A technique for quantifying heterogeneous ice nucleation in microlitre supercooled water droplets. *Atmospheric Measurement Techniques* **8**: 2437–2447. DOI: <https://doi.org/10.5194/amt-8-2437-2015>.
- Wheeler, PA, Watkins, JM, Hansing, RL.** 1997. Nutrients, organic carbon and organic nitrogen in the upper water column of the Arctic Ocean: Implications for the sources of dissolved organic carbon. *Deep Sea Research Part II: Topical Studies in Oceanography* **44**: 1571–1592. DOI: [https://doi.org/10.1016/S0967-0645\(97\)00051-9](https://doi.org/10.1016/S0967-0645(97)00051-9).
- Willis, MD, Leaitch, WR, Abbatt, JPD.** 2018. Processes controlling the composition and abundance of Arctic aerosol. *Review of Geophysics* **56**: 621–671. DOI: <https://doi.org/10.1029/2018RG000602>.
- Wilson, TW, Ladino, LA, Alpert, PA, Breckels, MN, Brooks, IM, Browse, J, Burrows, SM, Carslaw, KS, Huffman, JA, Judd, C, Kılıthau, WP, Mason, RH, McFiggans, G, Miller, LA, Nájera, JJ, Polishchuk, E, Rae, S, Schiller, CL, Si, M, Temprado, JV, Whale, TF, Wong, JPS, Wurl, O, Yakobi-Hancock, JD, Abbatt, JPD, Aller, JY, Bertram, AK, Knopf, DA, Murray, BJ.** 2015. A marine biogenic source of atmospheric ice-nucleating particles. *Nature* **525**: 234–238. DOI: <https://doi.org/10.1038/nature14986>.
- Wisecaver, JH, Hackett, JD.** 2011. Dinoflagellate genome evolution. *Annual Review of Microbiology* **65**: 369–387. DOI: <https://doi.org/10.1146/annurev-micro-090110-102841>.

- Xu, D, Kong, H, Yang, E-J, Li, X, Jiao, N, Warren, A, Wang, Y, Lee, Y, Jung, J, Kang, S-H.** 2020. Contrasting community composition of active microbial eukaryotes in melt ponds and sea water of the Arctic Ocean revealed by high throughput sequencing. *Frontiers in Microbiology* **11**: 1170. DOI: <https://doi.org/10.3389/fmicb.2020.01170>.
- Xu, H, Lv, H, Liu, X, Wang, PF, Jiang, H.** 2016. Electrolyte cations binding with extracellular polymeric substances enhanced *Microcystis* aggregation: Implication for *Microcystis* bloom formation in eutrophic freshwater lakes. *Environmental Science & Technology* **50**: 9034–9043. DOI: <https://doi.org/10.1021/acs.est.6b00129>.
- Xu, M, Tchinda, NT, Li, S, Du, L.** 2024. Enhanced saccharide enrichment in sea spray aerosols by coupling surface-active fatty acids. *Science of the Total Environment* **916**: 170322. DOI: <https://doi.org/10.1016/j.scitotenv.2024.170322>.
- Zábori, J, Krejci, R, Ekman, AML, Mårtensson, EM, Ström, J, de Leeuw, G, Nilsson, ED.** 2012a. Wintertime Arctic Ocean sea water properties and primary marine aerosol concentrations. *Atmospheric Chemistry and Physics* **12**: 10405–10421. DOI: <https://doi.org/10.5194/acp-12-10405-2012>.
- Zábori, J, Matisāns, M, Krejci, R, Nilsson, ED, Ström, J.** 2012b. Artificial primary marine aerosol production: A laboratory study with varying water temperature, salinity, and succinic acid concentration. *Atmospheric Chemistry and Physics* **12**: 10709–10724. DOI: <https://doi.org/10.5194/acp-12-10709-2012>.
- Zeppenfeld, S, van Pinxteren, M, Hartmann, M, Bracher, A, Stratmann, F, Herrmann, H.** 2019. Glucose as a potential chemical marker for ice nucleating activity in Arctic seawater and melt pond samples. *Environmental Science & Technology* **53**: 8747–8756. DOI: <https://doi.org/10.1021/acs.est.9b01469>.
- Zeppenfeld, S, van Pinxteren, M, Hartmann, M, Zeising, M, Bracher, A, Herrmann, H.** 2023. Marine carbohydrates in Arctic aerosol particles and fog—Diversity of oceanic sources and atmospheric transformations. *Atmospheric Chemistry and Physics* **23**: 15561–15587. DOI: <https://doi.org/10.5194/acp-23-15561-2023>.
- Zinke, J, Salter, ME, Leck, C, Lawler, MJ, Porter, GCE, Adams, MP, Brooks, IM, Murray, BJ, Zieger, P.** 2021. The development of a miniaturised balloon-borne cloud water sampler and its first deployment in the high Arctic. *Tellus B: Chemical and Physical Meteorology* **73**: 1–12. DOI: <https://doi.org/10.1080/16000889.2021.1915614>.

How to cite this article: Mirrielees, JA, Kirpes, RM, Costa, EJ, Porter, GCE, Murray, BJ, Lata, NN, Boschi, V, China, S, Grannas, AM, Ault, AP, Matrai, PA, Pratt, KA. 2024. Marine aerosol generation experiments in the High Arctic during summertime. *Elementa: Science of the Anthropocene* 12(1). DOI: <https://doi.org/10.1525/elementa.2023.00134>

Domain Editor-in-Chief: Jody W. Deming, University of Washington, Seattle, WA, USA

Associate Editor: Jeff S. Bowman, Scripps Institution of Oceanography, University of California San Diego, La Jolla, CA, USA

Knowledge Domain: Ocean Science

Part of an Elementa Special Feature: Insights into Biogeochemical Exchange Processes at Sea Ice Interfaces (BEPSII-2)

Published: October 22, 2024 **Accepted:** September 10, 2024 **Submitted:** December 01, 2023

Copyright: © 2024 The Author(s). This is an open-access article distributed under the terms of the Creative Commons Attribution 4.0 International License (CC-BY 4.0), which permits unrestricted use, distribution, and reproduction in any medium, provided the original author and source are credited. See <http://creativecommons.org/licenses/by/4.0/>.

